To the Graduate Council:

I am submitting herewith a thesis written by Helen M. Henson entitled "Morphology and Properties of Melt-Spun Polypropylene." I recommend that it be accepted in partial fulfillment of the requirements for the degree of Master of Science, with a major in Metallurgical Engineering.

J. E. Spruiell

Joseph E. Spruiell, Major Professor

We have read this thesis
and recommend its acceptance:

James L. Whitte

Edward S. Clark

Accepted for the Council:

L. Evans Roth

Vice Chancellor
Graduate Studies and Research

Thesis
79
.H458
cop. 2

MORPHOLOGY AND PROPERTIES OF MELT-SPUN POLYPROPYLENE

A Thesis

Presented for the

Master of Science

Degree

The University of Tennessee, Knoxville

Helen M. Henson

December 1979

1404976

Dedicated to

my father, my husband,

and my son

ACKNOWLEDGMENTS

The author gratefully acknowledges the guidance and support of Professor J. E. Spruiell throughout this research. The enthusiasm and cooperation of the entire faculty and staff of the Chemical, Metallurgical, and Polymer Science Engineering Department is appreciated. Acknowledgment is made to Dr. J. R. Dees who provided invaluable advice during the initial stages of this investigation, and to M. Hunter for aid in the measurement of mechanical properties.

The aid of personnel in the Chemical, Metallurgical, and Polymer Science Engineering Electronic and Machine shops is greatly appreciated. Recognition is given to Hercules, Inc., for supplying the polymer used in the study. Appreciation is expressed to the Department of Chemical, Metallurgical and Polymer Engineering for the financial aid provided.

The exceptional patience of the author's family is recognized; it was necessary for the completion of this work.

ABSTRACT

The purpose of this investigation was the experimental study of structural and morphological development during the melt spinning of an isotactic polypropylene and the correlation of developed structure and morphology with observed mechanical properties.

Experimental data was obtained from spinning apparatus consisting of an extruder-spin head mounted on a column so that data could be obtained from the moving spinline at specified distances from the spinneret. Measurements made included birefringence and surface temperature as well as x-ray diffraction.

Fibers were spun at three melt temperatures, and at varying take-up velocity. Spinning conditions were chosen so that the effect of stress and the effect of cooling rate could be treated separately.

Quantitative conclusions based on the experimental data have been made. At low measured spinline stress polypropylene fibers possess spherulitic morphology. As spinline stress is increased a "row structure" morphology is observed with chain or c-axis orientation becoming parallel to the fiber axis. This morphological change correlates with a change in fiber properties from "cold drawable" to "hard elastic."

The effect of bimodal chain or c-axis orientation on calculated Hermann-Stein orientation functions is shown.

Crystallization kinetics were observed to change with changes in both engineering stress and cooling rate. These changes could be discussed in terms of "constant cooling transformation" curves.

TABLE OF CONTENTS

CHAPTER		PAGE
I.	INTRODUCTION	1
II.	BACKGROUND OF RESEARCH	3
	A. Crystallization of Quiescent Melts	3
	Morphology	3
	Rate of Crystallization	6
	B. Crystallization of Isotactic Polypropylene	8
	Structure and Morphology	8
	C. Strain-Induced Crystallization	13
	Rate of Crystallization	13
	Structure and Morphology	14
	Bimodal Orientation	18
	D. Melt-Spinning	22
	The Melt-Spinning Process	22
	Modeling of the Process	22
	Structure Development During Melt Spinning	25
	Effect of Spinning Conditions on Structure and Properties of Fibers	27
III.	EXPERIMENTAL DATA COLLECTION AND ANALYTICAL PROCEDURES	33
	A. Data Collection	33
	Process Equipment	33
	Spinline Measurements	35
	Measurements Made of As-Spun Fibers	36
	B. Analytical Procedures	39
	Crystalline Orientation Functions	39
	Determination of Crystalline Fraction	46
	Orientation of Amorphous Regions	48
IV.	RESULTS AND DISCUSSION	50
	A. The As-Spun Filaments	50
	Crystalline Fraction	50
	Crystalline Orientation and Morphology	50
	Orientation of Amorphous Regions	59
	Mechanical Properties	59
	B. On-Line Studies of Spinning	62
	Crystallization Start Temperature	62
	Crystallization Kinetics	68
	The Development of Overall Orientation	74
	The Development of Crystalline Orientation and Morphology	74

CHAPTER PAGE

C. Discussion of Results 78
As-Spun Fiber Structure 79
Structure Development on the Spinline 81

V. CONCLUSIONS 83

A. As-Spun Filaments 83
B. On-Line Studies 84

LIST OF REFERENCES 85

VITA 89

LIST OF FIGURES

FIGURE		PAGE
1.	Morphological Units Within a Developing Spherulite	5
2.	Monoclinic Unit Cell of Isotactic Polypropylene	9
3.	Samuels Structure--Spherulitic Deformation Under Stress	15
4.	Row Structure	17
5.	Growth from an Oriented Thread of Polypropylene	19
6.	Functional Morphology of Elastic Polypropylene	21
7.	Spinning Apparatus	34
8.	Experimental Arrangement for Orientation Determination of Spun Fibers	38
9.	Geometry of a Pinhole Pattern	40
10.	Bimodal Orientation and Resultant Intensity	43
11.	Separation of Primary (C-Axis Oriented), Secondary (A-Axis Oriented), and Random Components	44
12.	Measurement of Crystalline Fraction	49
13.	WAXS and SAXS Patterns of Melt-Spun PP Filaments	52
14.	Crystalline Orientation Functions as a Function of Take-Up Velocity for Polypropylene Fibers Spun at Three Melt Temperatures	53
15.	Crystalline Orientation of Melt-Spun Fibers as a Function of Spinline Stress	55
16.	Relative Fractions of Primary (C) and Secondary (A) Components Versus Spinline Stress	56
17.	Crystalline Orientation of Melt-Spun Fibers (Neglecting A-Component) as a Function of Spinline Stress	58
18.	Birefringence of As-Spun Filaments and Contribution Due to Orientation of Amorphous Material as a Function of Spinline Stress	60

FIGURE PAGE

19. Typical Stress-Strain Curves Obtained from Fibers Spun at Low and High Spinline Stress 61

20. Elastic Recovery of Filaments as a Function of Spinline Stress 63

21. Mechanical Properties of Filaments as a Function of C-Axis Orientation 64

22. On-Line WAXS Patterns with Temperature and Birefringence Profiles for Melt-Spun Polypropylene Filament 65

23. Crystallization Start Temperatures on the Spinline as a Function of Spinline Stress 66

24. Measured Cooling Rate as a Function of Take-Up Velocity . . . 69

25. Crystallization Start Temperature Versus Stress at Several Cooling Rates 70

26. Crystalline Index as a Function of Spinline Residence Time from Analysis of WAXS Patterns 71

27. Crystallization Start Temperature as a Function of Cooling Rate for Quiescent and Stressed Melts 72

28. A Comparison of Spinline Crystallization Temperatures with Those Obtained upon Continuous Cooling of Quiescent Melts . . 73

29. On-Line WAXS and Temperature Profile for Melt-Spun Polypropylene Filament 75

30. Orientation Development on the Spinline 76

31. Relative Amount of Primary (C-Axis Oriented) and Secondary (A-Axis Oriented) Material as a Function of Spinline Residence Time 77

32. On-Line Development of Crystalline Orientation 78

33. Morphology of Polypropylene Melt Spun at High Stress 80

CHAPTER I

INTRODUCTION

The melt-spinning and subsequent drawing of synthetic fibers have been important commercial processes since the pioneering work of Carothers and Hill (9) in 1932. Although the structure and properties of drawn fibers have been the focus of much attention, it has also been realized that the properties of fibers, both before and after drawing, are dependent on the spinning conditions used in their manufacture. In fact, the application of this knowledge to the formation of useful fibers can be credited to a great extent with the development of their commercial market, now exceeding a billion pounds a year. Until recently, however, there has been comparatively little information in the open literature relating spinning variables to the structure and properties of as-spun fibers, and theoretical models of the melt-spinning process have, for the most part, emphasized the rheological and heat transfer aspects of the upper part of the spinline. (Some notable exceptions are discussed in the next section.)

This thesis represents one installment in a program being carried out at The University of Tennessee to study structure development during melt-spinning and subsequent drawing of several synthetic fibers, and the correlation of the mechanical properties of these fibers with structural observations. Related work on the melt-spinning of polyethylene includes studies by Abbott and White (1), and Dees and Spriuell (14, 15) on melt-spinning, and White, Dharod and Clark (54) on spin-draw

interaction. The present study is directed toward the correlation of spinning variables with developed structure in monofilaments of an isotactic polypropylene, as well as the study of structural formation using direct experimental measurement during the spinning process. Subsequent research by Nadella et al. (35, 36) extends the present study to include the effect of varying the molecular weight and tacticity on the structure and mechanical properties of both spun and drawn polypropylene.

CHAPTER II

BACKGROUND OF RESEARCH

A. CRYSTALLIZATION OF QUIESCENT MELTS

Morphology

The characteristic crystalline growth unit from a quiescent polymer melt is the spherulite; a structure showing radial polycrystalline growth from a single primary nucleus. The radiating crystals frequently branch in order to fill space so that density remains reasonably constant as growth proceeds. The formation of such structures is not limited to polymer melts, but is commonly observed when high viscosity of the melt limits diffusion so that nucleation and growth occur slowly (29).

A prominent feature of spherulites is the presence of the radiating crystal in fibrous or lamellar sub-units. Rapidly solidified melts grow fine fibrils, but this structure often coarsens during slower spherulitic growth. Keith and Padden (29) explain this phenomenon as a consequence of cellular branching. Low molecular weight or less tactic material tends to be rejected by the growing lamella and to form an "impurity"-rich layer in the melt at the liquid-solid interface. If the linear growth rate of the crystal is low this layer remains relatively thin, leading to a sharp gradient in transformation temperature at the interface and enhancing growth of projections from the surface. Cellulation occurs, and the fibrils branch and spread. The average width of the growing branches is proportional to $\delta = D/v$, where D is the diffusion

coefficient of the impurity in the liquid and v is the linear growth rate of the crystalline phase. Several investigators (20, 44) have suggested that branching occurs as growth from defects in the crystal structure of the lamellae. The lamellae are usually of the order of 100Å thick but may be several hundred or even thousands of angstroms in other dimensions. Within lamellae the polymer chains are parallel or nearly parallel to the shortest dimension--a consequence of growth by incorporation of folded chains (44).

Sharples (44) raises the possibility of initial spherulitic growth in the form of a single crystal, with the structure becoming polycrystalline only after branching sets in. Since the radial development of the spherulite depends on the nucleation density, he suggests that rod or plate-like crystallization modes may be an effect of limiting spherulitic growth.

In some polymers the fibrils or lamellae are observed to twist, and spherulites may show regular banding. This effect is frequently seen in polyethylene crystallization. The effect has been explained as a mechanism of relieving strain energy which is concentrated at the lamellar surface either by incorporation of impurities (29) or by the presence of chain folds (33).

After impingement the rejected material either crystallizes in a secondary process on the lamellar surfaces or remains as an amorphous component between crystalline regions (44). Figure 1 shows the morphological units within a developing spherulite (44).

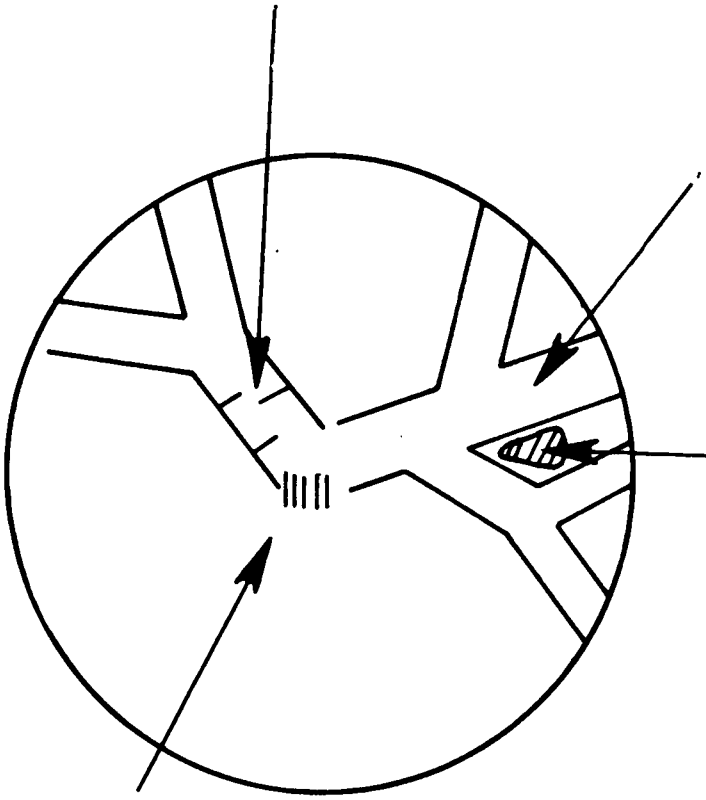

Figure 1. Morphological Units Within a Developing Spherulite.

Source: Sharples (44)

Rate of Crystallization

Isothermal crystallization kinetics may be studied using the Avrami equation

$$W/W_L = \exp(-zt^n)$$

where W/W_L is the weight fraction of liquid remaining after time t, z is a crystallization rate constant and n is the Avrami exponent. The value of n depends on the mechanism and shape of nucleation and crystal growth. Both nucleation rate and growth rate parameters are contained in z.

The overall rate at which the crystallization process occurs is a combination of both nucleation and growth rates. The maximum nucleation speed is normally found at a lower temperature than the maximum speed of growth. Thus, with small amounts of supercooling the crystallization rate is normally nucleation rate controlled; with large amounts of supercooling, the growth rate may control the crystallization rate.

In a homogeneous, supercooled liquid, stable nuclei exceeding a definite critical size (determined by a free energy change per unit volume and the creation of a surface free energy per unit area) must be formed so that crystallization will occur. Experiments by Mandelkern, et al. (33) performed just below the melting point, where nucleus formation plays a dominant role in crystallization kinetics, indicated that steady state nucleation and growth took place simultaneously throughout the crystallization process and that crystallization rates in the polymers examined could be satisfactorily discussed using conventional nucleation theory for long chain molecules.

Cormia, Price, and Turnbull (13) observed the freezing behavior of droplets of linear polyethylene under continuous cooling conditions and found that freezing occurred at much lower temperatures than commonly observed. They concluded that most polyethylene transformation involved heterogeneous nucleation. Devoy and Mandelkern (16) calculated the critical free energy for heterogeneous nucleation in conical cavities and on flat surfaces, and concluded that the free energy of formation was reduced relative to its value for homogeneous nucleation.

In 1949 Turnbull (49) discussed the effect of history on nucleation rate. He observed that the degree of supercooling required for crystallization depended on thermal history and suggested the possibility of embryonic structure retained above the melting point serving as sites for heterogeneous nucleation for subsequent solidification.

Extensive work has been done showing the effect of nucleating agents on crystallization rate. Beck and Ledbetter (6) demonstrated that the crystallization temperature of isotactic polypropylene was a function of concentration of the nucleating agent. Binsbergen (7) has studied the relative catalytic strength of various nucleating agents, and he has examined the temperature dependence of the nucleation process in the presence of nucleating agents.

The radius of a spherulite usually increases with the first power of the time until impingement. Sharples (44) interprets this observation as indicating the absence of a diffusion controlled process; the existence of a maximum in the curve of linear growth rate versus temperature he feels indicates growth limited by a process of secondary nucleation.

B. CRYSTALLIZATION OF ISOTACTIC POLYPROPYLENE

Structure and Morphology

Polypropylene is known to solidify from the melt with at least five ordered modifications.

The α form is the structure commonly observed when isotactic polypropylene is crystallized from the melt. Structure determination was carried out by Natta and Corradini (33). The unit cell possesses monoclinic symmetry. The values of the cell constants are

$$a = 6.65 \pm 0.05 \text{ Å}$$

$$b = 20.96 \pm 0.15 \text{ Å}$$

$$c = 6.50 \pm 0.04 \text{ Å}$$

$$\beta = 99°20' \pm 1°$$

and the polymer chains lie along the c axis. The identity period along this axis is 6.5 Å, indicating the presence of a threefold helical conformation of the molecule. The crystal lattice is centered with the most probable space group C_c. Figure 2 shows this monoclinic cell.

Natta and Corradini (33) report the existence of a smectic phase when molten polypropylene is quenched in water. (They state that the chains still possess threefold helical conformation but disorder exists in packking perpendicular to the chain axis.) Sheehan and Cole (11), in melt-spinning studies, found that increased cooling rate favored the formation of the smectic form.

The β form of polypropylene was first reported by Keith and Padden (28), who observed its sporadic appearance as two-dimensionally grown

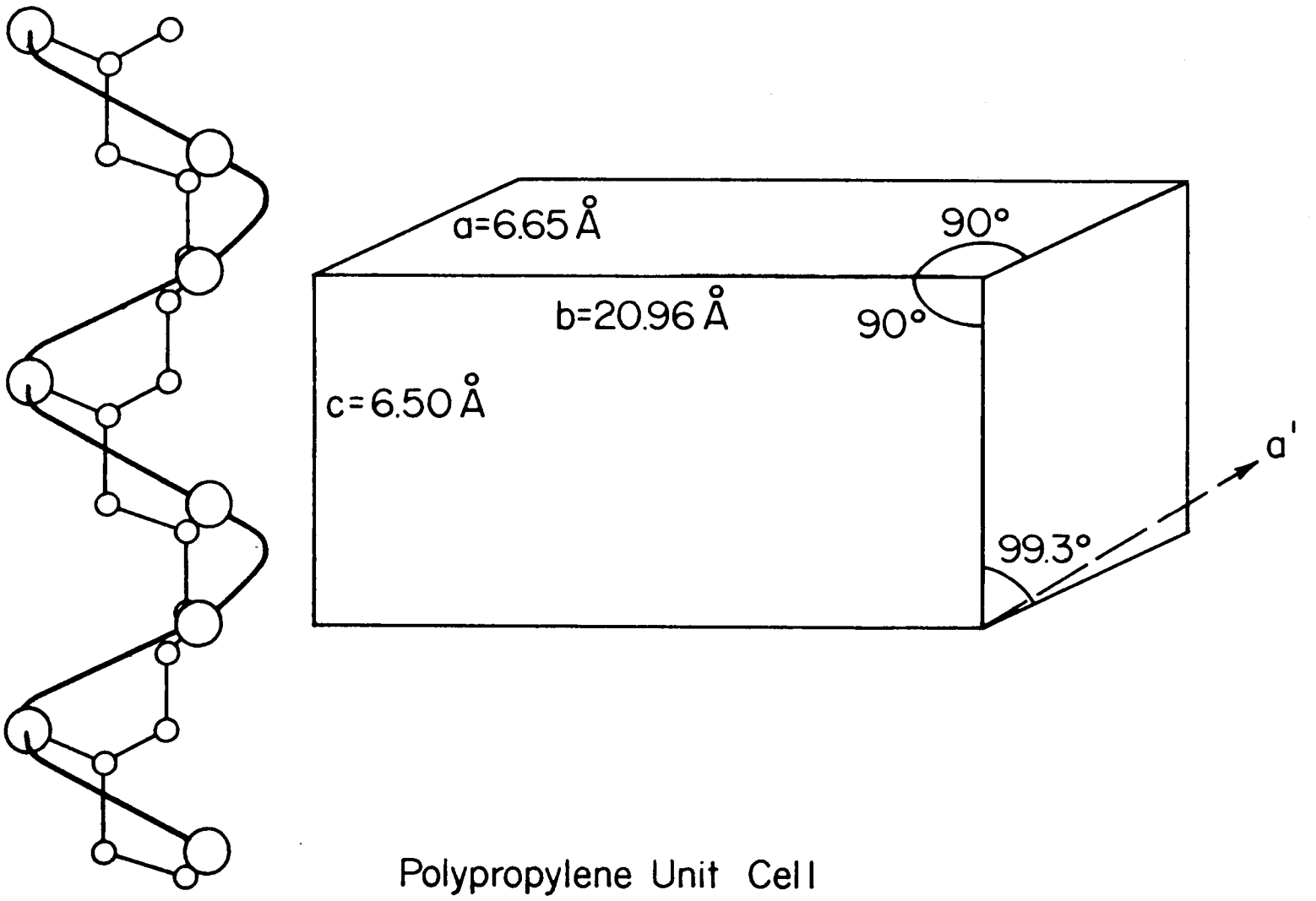

Figure 2. Monoclinic Unit Cell of Isotactic Polypropylene.

spherulites crystallized from the melt. They identified the structure as hexagonal. Turner-Jones et al. (50) obtained the β form by rapidly quenching the melt to below 130°C. Addink and Beintema (3) observed the β modification in fractions with a high degree of isotacticity. Samuels (40) heated Profax 6501 to ∿215°C for 10 minutes, and then allowed it to cool to room temperature at approximately 5°C per minute to obtain the β modification.

The γ modification is found on cooling fractionated polypropylene from the melt, as reported by Turner Jones (50) and Sauer (43). Kardos (17) reported the crystallization of whole polymer to γ phase when melts were solidified under pressure. The structure is thought to be triclinic.

The orthorhombic δ modification is observed only in specimens with a high percentage of amorphous material, separated from the bulk of isotactic material by extraction (3). Addink and Beintema suggest it may be a result of crystallizing a syndiotactic component.

We have observed only the α, or monoclinic, form in our fibers, and will restrict further discussion to that modification.

Padden and Keith (28) report two types of monoclinic spherulites differing only in the sign of their birefringence. Geil (20) suggests that differences may be due to form birefringence since the basic morphology of both types appears to be the same and x-ray diffraction shows identical structure.

Keith and Padden (28) report that the molecular chain axis is aligned at an angle of 65-70° to the spherulite radius, and the b axis

is tangential. They report a granular overgrowth that develops at temperatures above 140°C and persists to the melting point. Upon subsequent cooling it may crystallize.

Khoury (31), in studying the evolution of spherulites in solution from dendritic precursors, identifies the b axis as the direction of slowest crystalline growth.

Samuels (46) identifies the growth direction as the a-axis direction by x-ray diffraction studies of microtomed sections from three-dimensionally grown spherulites.

C. W. Hock (22) used electron microscopy to characterize the morphology of polypropylene crystallized from the melt. Isothermally crystallized polypropylene was oxidized with nitric acid to release spherulites. These spherulites were then broken up into lamellae consisting of short chains whose length was measured by intrinsic viscosity measurements. The chains were found by electron diffraction to be perpendicular to the base of the lamellae, so calculated lamellar heights were obtained from the viscosity measurements. These heights were found to decrease with decreasing crystallization temperature.

Crystallization rates of isotactic polypropylene were studied by Hoshino et al. (23) for fractions with varying tacticity using dilatometric techniques. Induction times showed a similar variation with supercooling for the three tacticities studies. When the samples were cooled so that similar induction times were obtained, ultimate crystallinity varied directly with tacticity.

Radial growth rates, as determined by microscopy, were seen by Keith and Padden (29) to decrease with decreasing tacticity. In the

same study they showed radial growth rate increased with decreasing crystallization temperature, and remained constant in time.

C. W. Hock (22) reports, using optical microscopy, that radii of polypropylene spherulites decrease rapidly with decreasing crystallization temperature. In material crystallized isothermally at 145°C, 135°C, and 125°C, spherulites were well formed and had radii of 450 μm, 275 μm, and 175 μm, respectively. Since radial growth rate is increasing in this region, nucleation density must increase rapidly with supercooling.

No background data is apparently available on the effect of varying the molecular weight upon the crystallization kinetics of polypropylene.

Extensive work has been done on the effect of adding nucleating agents to polypropylene melts. Beck and Ledbetter (6) reported extraneous nucleation reduced spherulite size while increasing ultimate crystallinity. They found an increase in crystallization rate with the addition of nucleating agents at all temperatures studied. A dependence of crystallization temperature on the concentration of nucleating agent was observed, with the dependence becoming weaker at high agent concentration.

F. L. Binsbergen (8) concluded that most polypropylene nucleating agents were composed of rows or layers of molecules, and that orientation of these nucleii led to a form of oriented crystallization.

Depth (size)
go to p. 13

C. STRAIN-INDUCED CRYSTALLIZATION

Rate of Crystallization

The discovery that natural rubber would crystallize under deformation may have been the stimulant for further studies of strain-induced crystallization. In a thermodynamic study, Flory (17) related the rise in the crystallization temperature to the degree of stretching of vulcanized rubber. Yamamoto and White (58) have developed a treatment for strain-induced crystallization of elastomeric network polymers.*

Haas and Maxwell (21) have made a quantitative study of the effect of shear stress on the crystallization rate of linear polyethylene. Their results indicated that crystallization half times were an order of magnitude lower for stressed material than for polyethylene crystallized under quiescent conditions.

Shii and Ishekawa (46) observed stress levels in irradiated polypropylene films held at constant strain as they cooled from the melt. Their data indicated both a decrease in induction time and an increase in crystallization rate with increasing extension.

In recent work, to be discussed in the next section, Katayama (25) and Dees and Spruiell (15) have studied crystallization rate during melt spinning, and concluded that melt orientation increased the overall rate of solidification.

---

*It is not entirely clear whether it is more appropriate to use the term "strain-induced" or the term "stress-induced." Both appear in the literature in reference to similar phenomena. The central idea is that molecular orientation is created and can lead to nucleation of crystals before relaxation by diffusion processes.

Structure and Morphology

Symmetrical spherulites are not characteristic of solidification from the melt under forces which tend to affect the orientation of the polymer chains. In 1966, Binsbergen (7), using a hot stage microscope, observed crystalline growth from sharp nucleating lines in the direction of shear as his samples slowly cooled under stress. Birefringence indicated that the polymer chains were aligned parallel to the direction of shear in the nucleating structure. Upon thermal cycling to 210°C, these nuclei reappeared as the sample cooled, and did not permanently disappear until the polypropylene was heated above 240°C. Binsbergen remarked on the similarity between these structures and the stirrer-induced crystalline structures formed by Pennings.

Samuels (40) has studied the structure of melt-spun polypropylene fibers, using the microtomed section of a three-dimensional spherulite as a model. He interprets the structures formed as a result of deformation on spherulites, where stress on the structure creates a yield region and corresponding molecular alignment with the polymer chains. This rather complex structure is shown in Figure 3.

In 1967 Keller and Machin (30) studied the structure of melt-extruded polyethylene sheet with x-ray diffraction. They brought forward the following hypothesis:

1. Row nucleation as the basic process of crystallization under stress. The proximity of the nucleii along the row confines crystal growth to the direction perpendicular to the direction of stress.

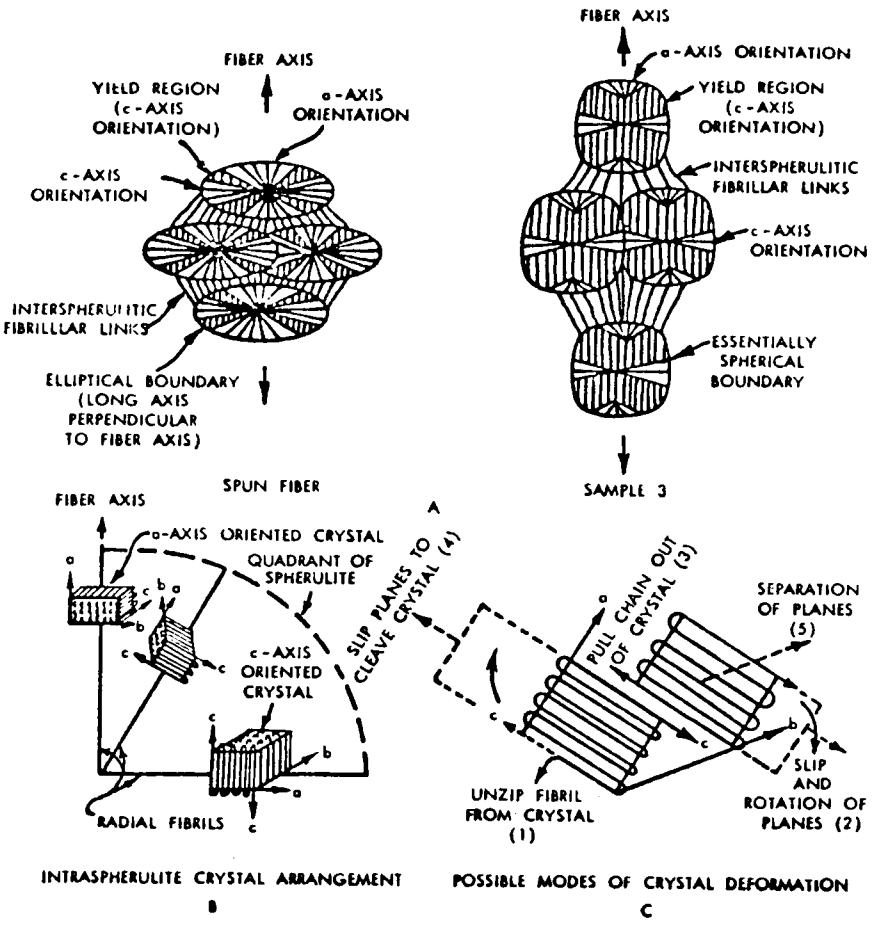

Figure 3. Samuels Structure--Spherulitic Deformation Under Stress.

2. If stress is small then crystals will grow as they do in spherulites (i.e., they twist). At higher stress the chain axes become aligned in the stress direction.

The characteristics of this structure as seen by x-ray diffraction are:

1. alignment of the b axis or growth direction perpendicular to the direction of stress while the c and a axis orientation remain relatively unoriented as the twisted growth from row nucleii begins, and
2. an increase in the alignment of the c axis with the fiber axis with less twisting of the lamellae.

Katayama and co-workers (26) have observed highly oriented stacking of lamellae perpendicular to the deformation direction in electron microscopy of polypropylene film crystallized from sheared polymer melts, as well as on the surface of polyethylene melt-spun fibers. Small angle x-ray diffraction patterns show the meridional maxima characteristic of a lamellar structure.

Other investigators (52, 47, 38, 26, 27) confirm the existence of these meridional maxima in small angle patterns of material crystallized under stress. An anomoly is reported by Weidinger and Hermans (52) who show discrete reflections on the equator in SAXS patterns of highly oriented melt-spun polypropylene fibers.

Clark and Garber (10) suggested that a row structure morphology be used as a model to predict properties of highly elastic fibers. Such a row structure is shown in Figure 4. Clark (11) proposed that the

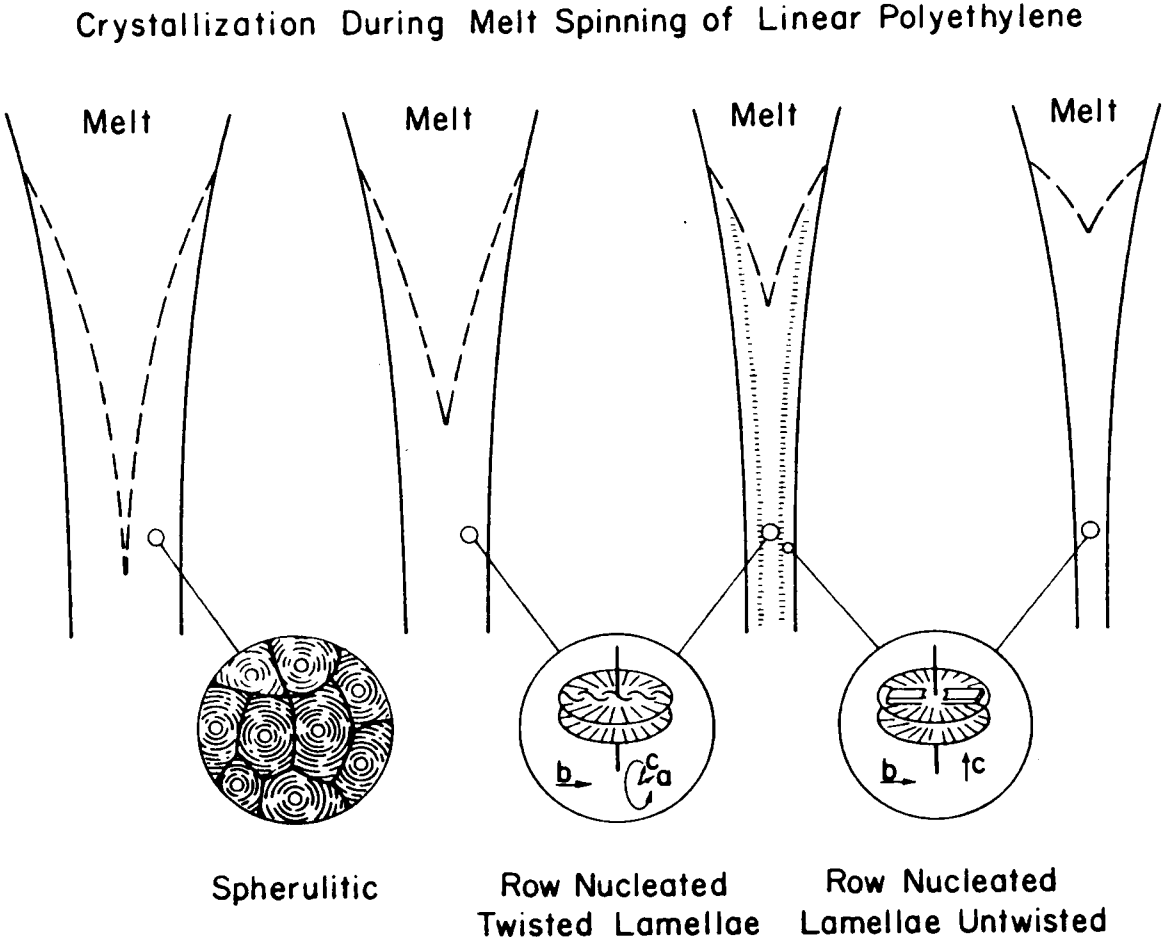

Figure 4. Row Structure.

Source: Dees and Spruiell (15)

deformation mechanism is that of bending or shearing lamellae connected with tie molecules. Measurements of high pressure mercury porosimetry, small angle x-ray diffraction and specific volume support his claim.

Fung and Carr (19) interpret a varying birefringence across spun fibers of polyethylene and polypropylene in terms of row structure.

An interesting illustration of two-dimensional polypropylene growth from a fibril nucleus has been produced by Geil (20), and is reproduced in Figure 5. This illustration seems consistent with a row structure.

Bimodal Orientation

Several patents have been based on the unusual dual orientation of the polymer chain axes found in polypropylene crystallized under stress. Examples include "highly elastic" polypropylene fibers, as well as films and injection moldings. "Bimodal," "binodal," or biaxial orientation of monoclinic polypropylene may be recognized by the two maxima in the 110 Debye ring of the WAXS pattern. It consists of two monoclinic crystalline populations; the first, or C, population having polymer chain axes parallel to the stress direction, the second or A, population with chain axes perpendicular to the direction of stress.

At least three morphological models have been proposed to describe the morphology of polypropylene having this double orientation. Samuels (40) describes the separation as the result of lamellar bending in the polar region of the deformed spherulite mentioned previously and shown schematically in Figure 3. An alternative model proposed by Clark and Spruiell (12) consists of a primary row structure with growth occurring

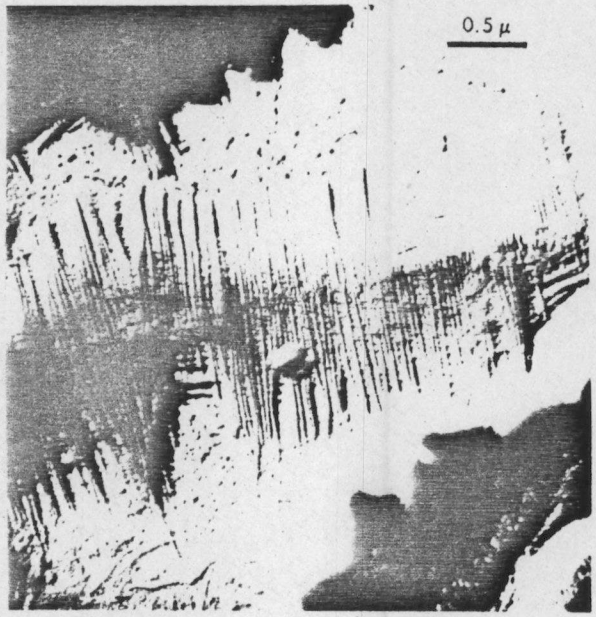

Figure 5. Growth from an Oriented Thread of Polypropylene.

Source: Geil (20)

along the a' axis of the pseudo-orthorhombic unit cell. Chains rejected from this primary structure then crystallize epitaxially on the surface of the previously formed lamellae. Clark and Spruiell suggest that this secondary population may act as a cushion which distributes stress evenly among interlamellar links upon extension. The epitaxial attraction between components would serve to keep the cushion in place. They find this morphology, shown in Figure 6, compatible with the considerable stress life of the polypropylene molded-in hinge.

Considerable support for this model comes from Katayama and co-workers. In melt spinning studies to be discussed in a later section, Katayama et al. (25), reports the appearance of the primary component before the secondary, consistent with the concept of an overgrowth. Dark field electron microscopy showed the lamellae to consist of the primary populations; but Katayama was unable to locate the secondary population regions, and suggested that they were too small to resolve. The crystalline imperfections expected within the secondary crystallite component, as well as small crystallite size would correlate with the broad secondary population x-ray diffraction peaks observed by Katayama.

A third possible morphology is suggested by results published by Geil (20, and structural studies of Khoury (31). Crystalline growth from a fibril nucleus showed a cross-hatched morphology, as shown previously in Figure 5. Similar lamellar structures in spherulitic precursors, described by Khoury, also possess a cross-hatch texture, this oriented growth would be consistent with the bimodal orientation diffraction pattern.

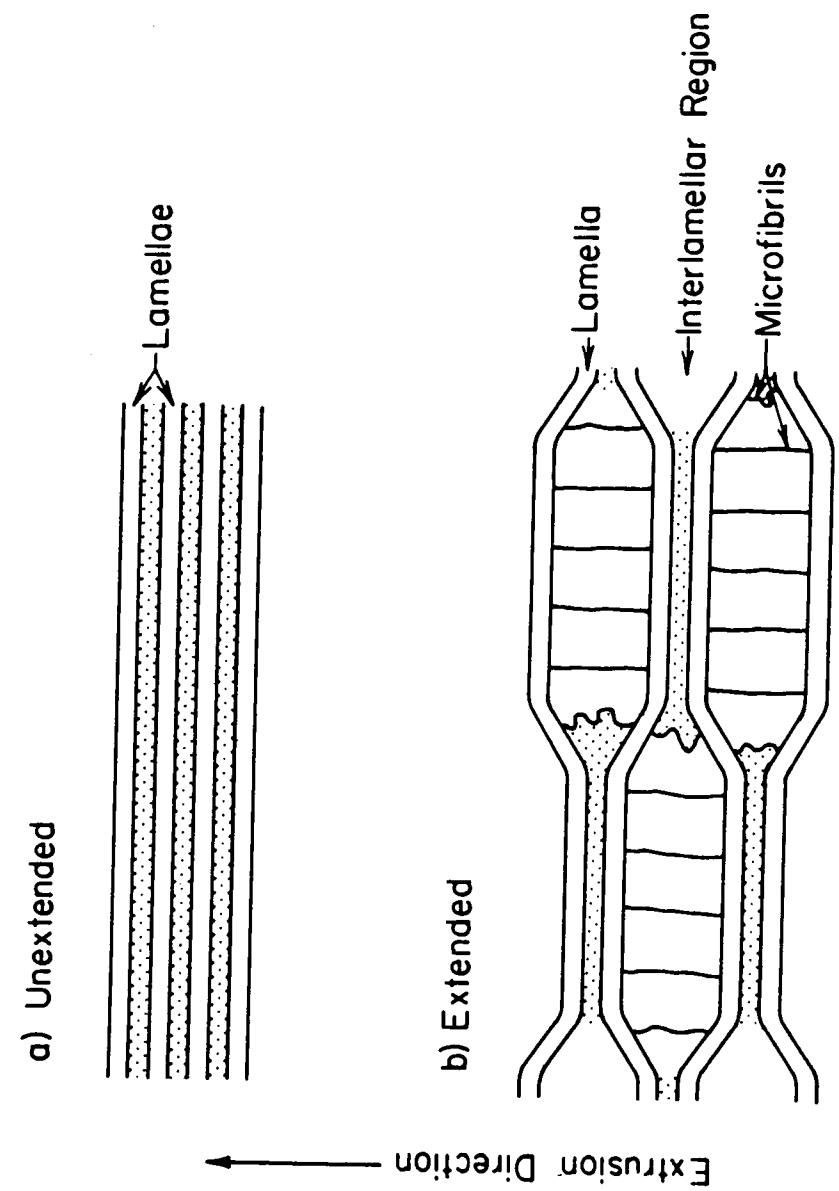

Figure 6. Functional Morphology of Elastic Polypropylene.

Source: Sprague (47)

D. MELT-SPINNING

The Melt-Spinning Process

The process of melt-spinning, first described by Carothers and Hill (9), involves crystallization under unaxial stress at high cooling rates. Polymer is fed to a heating chamber and the molten material is extruded through a small orifice, sometimes via a metering pump to keep flow constant. The emerging melt is drawn down, then solidified, as it moves through a cooling medium and is collected on a take-up device.

Because of the complex nature of the melt-spinning process, there are numerous process variables. Ziabicki (62) divides process variables into three groups:

1. primary variables: spinneret dimensions and number of holes in the spinneret, extrusion temperature, mass flow rate, take-up velocity, and cooling conditions.
2. secondary variables: extrusion velocity, filament diameter, denier and deformation ratio.
3. resultant variables: tensile force and stress, final filament temperature, and structure.

It has long been known that varying the spinning parameters alters the properties of the spun fiber.

Modeling of the Process

A great amount of work on the modeling of the melt-spinning process has been done by Ziabicki (60, 62), who in 1960 and 1961 derived equations for velocity and diameter of the moving filament:

$$v/v_o = \exp\left(\frac{-F}{w}\int \rho/2\eta_e \, dx\right)$$

where v and v_o are velocity and spinneret velocity, ρ is density, F is tensile force, w is mass flow rate and η_e is Trouton viscosity.

$$d/d_o \simeq \left(\exp \; -\rho\frac{F}{w}\int_o^L \frac{dx}{\eta_e}\right)$$

where d and d_o are diameter and diameter at the spinneret, respectively.

Kase and Matsuo (27) extended the work of Ziabicki to cover transient conditions. They derived a set of partial differential equations for the basic physical balances on the spinning fiber.

$$\text{Force:} \quad \frac{dv}{dx} = F/\eta_e A$$

$$\text{Material:} \quad v\frac{dA}{dx} + \frac{dA}{dt} = -A\frac{dv}{dx}$$

$$\text{Heat:} \quad v\frac{dT}{dx} + \frac{dT}{dt} = \frac{2\sqrt{\pi h}(T-T^*)}{\rho C_p \sqrt{A}}$$

where h is coefficient of heat transfer at the filament surface, T* is temperature of the cooling medium and C_p is the specific heat of the molten filament.

Several investigators, including White (53), and Acierno and co-workers (2), extended the analyses of the molten spinline from Newtonian to viscoelastic fluids. Acierno et al. (2) melt-spun filaments into an isothermal chamber as well as into ambient air in order to separately treat rheological and heat transfer phenomena.

In polymers such as polyethylene and polypropylene, as the fiber cools, crystallization occurs. In a simplified treatment of non-isothermal crystallization, Ziabicki (61) assumes that the rate of transformation, dx/dt, can be described with the aid of a first order kinetics equation

$$[1/(1 - X)]\frac{dx}{dt} = K(T)$$

where the rate constant K is a function of time-dependent temperature. The solution of this equation may be approximated

$$X(t) \simeq 1 - \exp\left\{-\int_{o}^{t} K[T(t)]dt\right. \quad ,$$

hey- you are pretty damn sexy, ya know that? Goto page 69.

$$= 1-\exp\left[-\int_{T(t=0)}^{T(t)^{o}} K(T)\xi^{-1}dT\right.$$

where $\xi = \frac{dT}{dt}$ or cooling rate. Since crystallization occurs between the melting point and glass transition temperature, Ziabicki defines a "kinetic crystallizability" as

$$G = \int_{Tg}^{Tm} K(T)dT$$

and the final degree of crystallinity may be expressed as

$$X_f = 1 - \exp(G/\xi)$$

Structure Development During Melt Spinning

There has been some study of crystallization and structure formation in the spinline. Abbott and White (1) report the results of a study to characterize the rheology and structure formation of melt-spun polyethylene, and in addition to correlate the mechanical properties of the filaments to spinning conditions through the crystallinity and orientation developed during the process. They concluded (for HDPE) that with increasing draw-down, the level of crystallinity decreased, and crystalline orientation increased. Elastic modulus, tensile strength, and elongation to break were observed to correlate with crystalline orientation.

In a study involving a linear polyethylene, isotactic polypropylene, as well as isotactic polybutene-1, Kitao et al. (32) investigated the effect of melt-draw ratio on the orientation of both the crystalline regions and amorphous regions. Similar results are reported for crystalline orientation of both polyethylene and polypropylene, with birefringence and crystalline orientation functions varying with melt-draw ratio. It was concluded that polyethylene and polypropylene crystallize in essentially identical manner, despite differences in chemical structure, crystal system and chain conformation, and Kitao remarks that the crystalline orientation functions seem to suggest the twisting lamellar structure described by Keller.

A study of structural development in fibers of polyethylene, polypropylene and polybutene-1 was made by Katayama et al. by obtaining

experimental measurements on a moving spinline. Fiber diameter, birefringence and surface temperature data, as well as wide and small angle x-ray diffraction patterns, were obtained as a function of distance from the spinneret. Katayama et al. observed increasing birefringence and plate-like density variations as shown by small angle x-ray diffraction in the spinline in the region just before the first crystalline reflections are observed. Small and wide angle diffraction patterns taken along the spinning way show high orientation of the chain axes and lamellae normal to the fiber axis in the first structures to form. As crystallization progresses, less orientation of the crystalline phase is observed. Birefringence measurements supported these observations. Katayama interprets this data in terms of the high stress conditions under which solidification first occurs. The first crystalline reflections were observed just before the filament reached its final diameter. Crystallization half times were observed to decrease with increasing take-up velocity.

Similar results were reported for polypropylene. The first crystallites to form are oriented with chain axes parallel to the fiber axis. Later in the crystallization process a second population appears with chain axes normal to the fiber axis. Unlike polyethylene, crystallization occurred sometime after the filament has reached its final diameter for the set of spinning conditions shown.

The development of crystallinity in a moving polyethylene spinline, and the correlation of the observed structure with mechanical properties of the fiber has been the subject of a recent comprehensive study by

Dees and Spruiell (15), at The University of Tennessee. Equipment and procedures developed by these authors for the study of polyethylene were subsequently employed for this present polypropylene study, and are described in the following section.

Effect of Spinning Conditions on Structure and Properties of Fibers

Dees and Spruiell observed that variation in fiber orientation with such variables as take-up velocity, mass flow rate, and melt temperature could be largely traced to the effect that such variables had on spinline stress, and that molecular orientation, both within the crystalline regions and of the overall fiber, could be expressed as a function of spinline stress. The Hermans' orientation functions of the crystalline axes showed variation with increasing spinline stress as follows:

1. a transition from spherulitic to row-nucleated structure with regularly twisting lamellae, and
2. untwisting of the lamellae to align the molecular chains with the fiber axis.

The variation in crystalline orientation along the spinline was seen to depend on the overall spinline stress. At very low and very high stress levels the first crystals to appear have orientation similar to those of the final fiber. However, at intermediate stress levels the first crystallization shows relatively high molecular chain alignment with the fiber axis, with overall orientation decreasing as crystallization proceeds, in a manner similar to that observed by Katayama. This phenomenon is explained as follows:

In the intermediate range of take-up velocities crystallization begins near the relatively cool filament surface. The slightly lower temperature results in higher viscosity and stress in this region and promotes the formation of untwisted lamellae. This fiber skin layer supports most of the load so that subsequent crystallization occurs toward the interior of the fiber at lower stress levels. The overall effect is a decreasing molecular orientation in the crystalline region with developing crystallinity.

The first crystalline reflections were consistently observed at a point just before the fiber reached its final diameter (i.e., at the peak of the linear fiber velocity gradient). Crystallization rates were found to be several orders of magnitude larger on the spinline than observed under quiescent condition, and are in reasonable agreement with those observed by Haas and Maxwell (21). Transformation temperatures were higher on the spinline than those obtained under quiescent conditions at much slower cooling rates, showing the effect of orienting stress. However, increasing take-up velocity lowered transformation temperature, and this was thought to show the effect of increased cooling rate with take-up velocity.

Birefringence of the fiber was found to be due almost entirely to the crystalline regions. Tensile strength, Young's modulus, and elongation to break were found to correlate with crystalline orientation function, as well as with spinline stress.

The effect of spinning variables on the structure and properties of isotactic polypropylene has been the subject of several investigations.

In 1964 Sheehan and Cole (45) reported the production of high-tenacity polypropylene filaments. They reported that the wide-angle diffraction patterns obtained from the as-spun filaments depended on

1. melt temperature,
2. spin-draw ratio, and
3. quench employed.

They found that while holding the other variables constant, increasing the melt temperature or decreasing the quench temperature would change the structure from crystalline to paracrystalline. Decreasing melt temperature changed randomly oriented crystalline structure to one in which the molecular chains tended to be parallel to the fiber axis, and increasing spin-draw ratio oriented both crystalline and paracrystalline structures. The crystallinity, as measured by density, remained nearly the same for all as-spun filaments. Stretching during spinning affected the tenacities of the drawn fibers with high spin-draw ratios reducing tenacity after drawing. Plots of tenacity versus orientation angle after drawing showed that tenacity increased more rapidly with orientation for filaments spun to produce relatively little orientation than those showing high orientation in the as-spun condition. Sheehan and Cole suggest differences other than orientation in the crystalline phase of the melt-spun fibers.

Baranow (5) and Volkov (51) used small-angle light scattering, birefringence measurements and wide-angle x-ray diffraction to characterize morphology as a function of melt temperature, draw ratio, and, in addition, of local heating of the spinneret. They divided the fiber

into two phases--a deformed spherulitic component, and an amorphous component which contained an "oriented phase."

Baranov explains the stretching of the spherulite as an effect of the mechanical gradient in the spinline, while Volkov postulates a relaxation phenomenon. The spherulitic radius, R, was found to be related to the fiber diameter d by the equation

$$R = k\ (d - d_o)$$

where d_o is a function of the local heating of the spinneret, and d, the final fiber diameter is a function of the draw ratio. The spinning of a fiber where $d = d_o$ and spherulitic radii disappeared implied an increase of the melt-draw ratio. The birefringence of the sample was calculated to saturate at the same drawdown ratio corresponding to $d = d_o$. At constant drawdown ratio, spherulitic radius was seen to decrease with spinneret temperature.

B. S. Sprague (38,47) and colleagues at Celanese Research Corporation have correlated the observed structure and morphology of "hard elastic" fibers, such as polypropylene with their mechanical and physical behavior. Sprague relates the effect of fiber formation conditions and annealing to the observed structural features of the fiber, then goes on to propose a morphological model relating these features to the observed mechanical properties.

"Hard elastic" fibers are characterized as showing, after special annealing, high recovery from very high strains, reversible reduction of

density with a large increase in pore volume, a negative temperature coefficient of retractive force on stretch materials and high deformability at liquid nitrogen temperature. The structural features observed in fibers encompass a wide range from low crystalline and lamellar order to stacked lamellar aggregates and high molecular orientation as seen by x-ray diffraction.

Annealing is seen to increase both crystalline and lamellar order as well as to increase the long period of the melt-spun fibers. Electron microscopy of annealed polypropylene film revealed uniform lamellae oriented normal to the extrusion direction. Extension of 50% shows non-uniform variation in long period. Some areas show cracks between lamellae that are bridged by microfibrils.

The model proposed is similar to that shown in Figure 6 (page 21). As the structure is extended, the tendency of the lamellae to stick together must be exceeded by a specific stress, the yield stress, and the lamellae separated before elastic spring action is evident. Figure 6 also suggests that tie molecules play a role in limiting the extension.

In two studies discussed previously, Abbott and White, and Dees and Spruiell found that elastic modules and tensile strength of as-spun filaments increase with crystalline orientation while the elongation to break decreased. Dees and Spruiell observed that this correlation could also be made with spinline stress. Increasing stress changed morphology from spherulitic to row structure.

The important role of spinning variables on fiber structure and properties was illustrated in a series of patent applications filed in

1962-1968 for polypropylene, for fibers having high elasticity with useful resistance to elongation. Examples of various spinning conditions and the resultant crystalline orientation, as shown by wide-angle x-ray diffraction, as well as effects on physical properties are described.

CHAPTER III

EXPERIMENTAL DATA COLLECTION AND ANALYTICAL PROCEDURES

A. DATA COLLECTION

Process Equipment

Figure 7 is a schematic diagram of the equipment used to spin filaments and to obtain experimental data on a running spinline. The extrusion spinning apparatus, manufactured by Fourné Associates in West Germany, to University of Tennessee specifications, consisted of a 13 mm screw extruder used to feed the molten ploymer at constant pressure to a metering pump. The pump discharge provided a steady flow rate through a single capillary spinneret 0.762 mm diameter by 3.81 mm long. This equipment was mounted on a threaded column so that the spinneret could be moved vertically with respect to the platform on which the entire assembly was positioned.

Polymer flow rate through the spinneret was held constant at 2 gms per minute by a gear type metering pump. The extruder screw speed was varied to obtain constant pressure between the extruder and the metering pump. This pressure was sensed by a liquid bulbtype transducer, and indicated by a Bourdon gauge.

Melt temperature of the polymer was maintained by controlled electrical band heaters, and was measured by platinum resistance thermometers in the discharge from the extruder and from the metering pump. Polypropylene melt temperatures of 260, 230, and 200°C were employed.

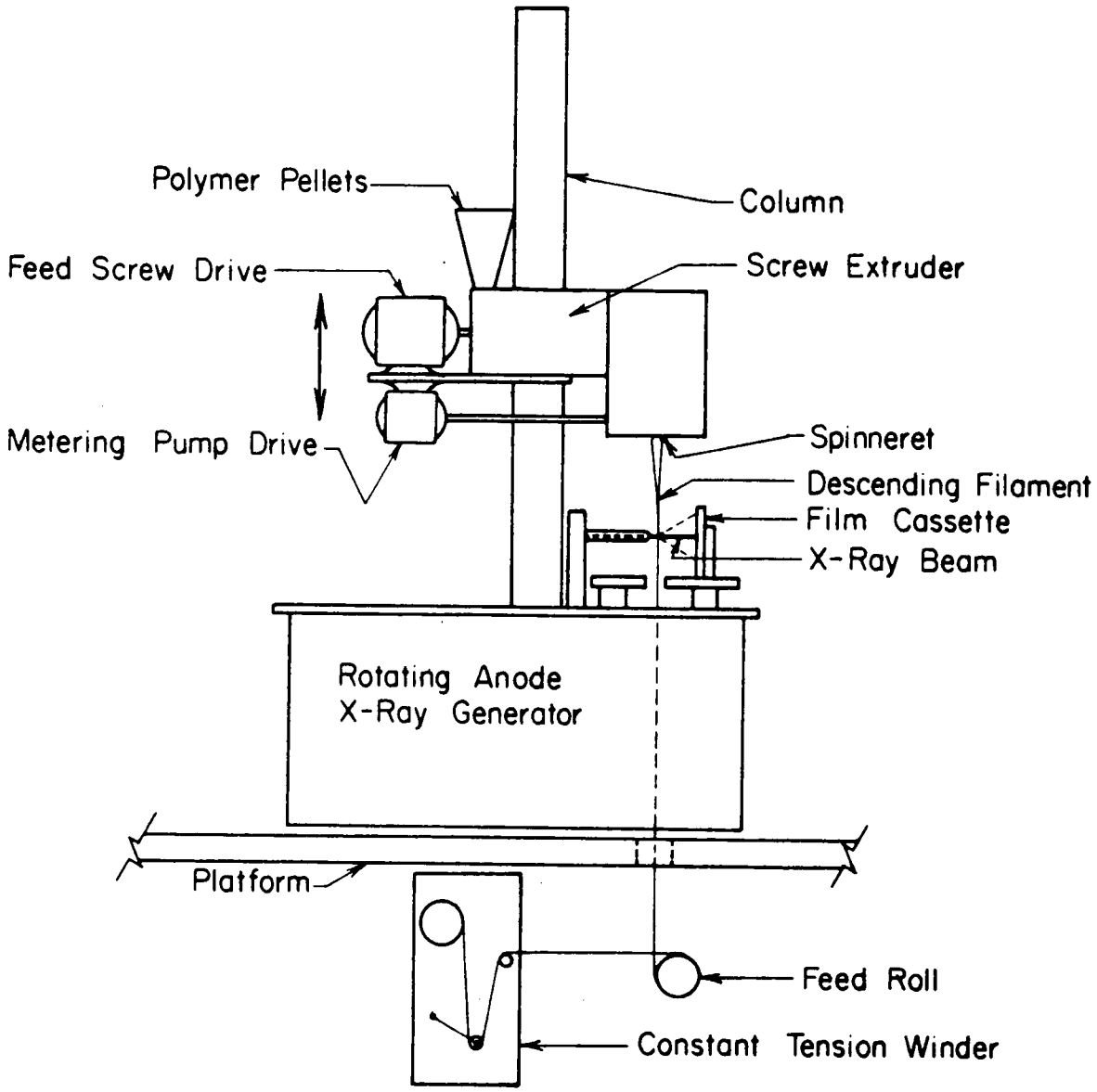

Figure 7. Spinning Apparatus.

The monofilament was taken up below the equipment platform on a Leesona 955 constant tension winder. Uniform take-up velocity was maintained by passing the spinline one full turn around a cardboard bobbin mounted on a direct current motor driven by a Heller controller. Linear fiber speeds ranged from 25 to 550 meters per minute. The resultant filament tension was determined using a Rothschild tensiometer equipped with a ten gram measuring head mounted directly above the feed roll, and was corrected for diameter variations. Overall spinline stress was calculated from the tension and the diameter of the spun filament; it varied from 8×10^5 to 33.4×10^6 dynes per square centimeter.

All work was done using highly isotactic Hercules Profax 6423 polypropylene with melt index 6.9 gms/min. Molecular weight, as determined by Nadella (35) from intrinsic viscosity measurements was 2.8×10^5.

Spinline Measurements

Experimental measurements obtained as a function of distance from the spinneret consisted of the (a) wide-angle x-ray diffraction pattern, (b) temperature, (c) diameter, and (d) birefringence of the spinning filament. Measurements were made at three melt temperatures, 260°, 230°, and 200°C at take-up velocities from 25 m/min to 550 m/min.

Wide-angle x-ray diffraction. A hole in the chassis of a Rigaku-General Electric rotating anode x-ray generator permitted passage of the filament through a collimated x-ray beam. CuK_α radiation generated with 50 kV electrons, target current 80 milliamps, was employed and the

resultant pattern was recorded on x-ray film placed 2 centimeters behind the moving filament. Exposure times under these conditions were strongly dependent on the filament diameter and varied from 15 minutes to 2 hours.

Temperature. Measurements of filament surface temperature were made using a Hastings-Raydist Match-Temp pyrometer coupled to a Leeds and Northrup potentiometer. The technique consisted of adjusting the calibrated temperature of the heated thermocouple bead until no heat flow was detected when the bead touched the moving filament.

Diameter. A 35 mm Nikon single-lens reflex camera equipped with bellows was used to photograph the spinline. The negatives obtained were projected on a screen and filament diameter compared with a standard scale, which was similarly photographed and projected.

Birefrigence. An Olympus model polarizing microscope equipped with compensator was mounted on the spinline so the spinning filament passed between crossed polars. Retardation measurements were made at magnifications of 50 and 100X; birefringence was calculated using spinline diameter measurements.

Measurements Made of As-Spun Fibers

Experimental measurements obtained consisted of (a) small-angle x-ray diffraction, (b) wide-angle x-ray diffraction, (c) density, (d) diameter, (e) birefringence, and (f) mechanical property measurements.

Small-angle x-ray diffraction. Small-angle x-ray diffraction patterns were obtained from a bundle of parallel filament clamped in a specimen holder and placed in a Kiessig camera mounted on the

Rigaku-General Electric generator. Sample thickness was an estimated 3 mm, sample-to-film distance was 40 cm. Exposure times were in the range of 1 to 2 hours, using the generating conditions previously described. The collimator for the x-ray beam was designed so that the camera had a resolution of approximately 400Å. During operation the camera was evacuated with a mechanical pump to eliminate scattering from air molecules.

Wide-angle x-ray diffraction. Wide-angle x-ray diffraction measurements were made using a diffractometer in order to get quantitative measurements of the preferred orientation. The experimental arrangement is illustrated in Figure 8. Filaments were wrapped around the sample holder to form a plane of parallel fibers. This holder was positioned to bisect the angle between the incident beam and the detector. Rotation brought the fiber axis from normal to parallel with the diffracting planes.

Density. Filament density was measured in a distilled H_2O-methanol density gradient column.

Diameter and birefringence. The Olympus polarizing microscope with filar eyepiece was removed from the spinline for diameter and retardation measurement of the as-spun fibers.

Mechanical properties. Force-versus-elongation curves were obtained at room temperature using an Inston tensile tester at a cross-head speed of 2 in./minute. Yield strength, tangent modulus and elongation to break were measured.

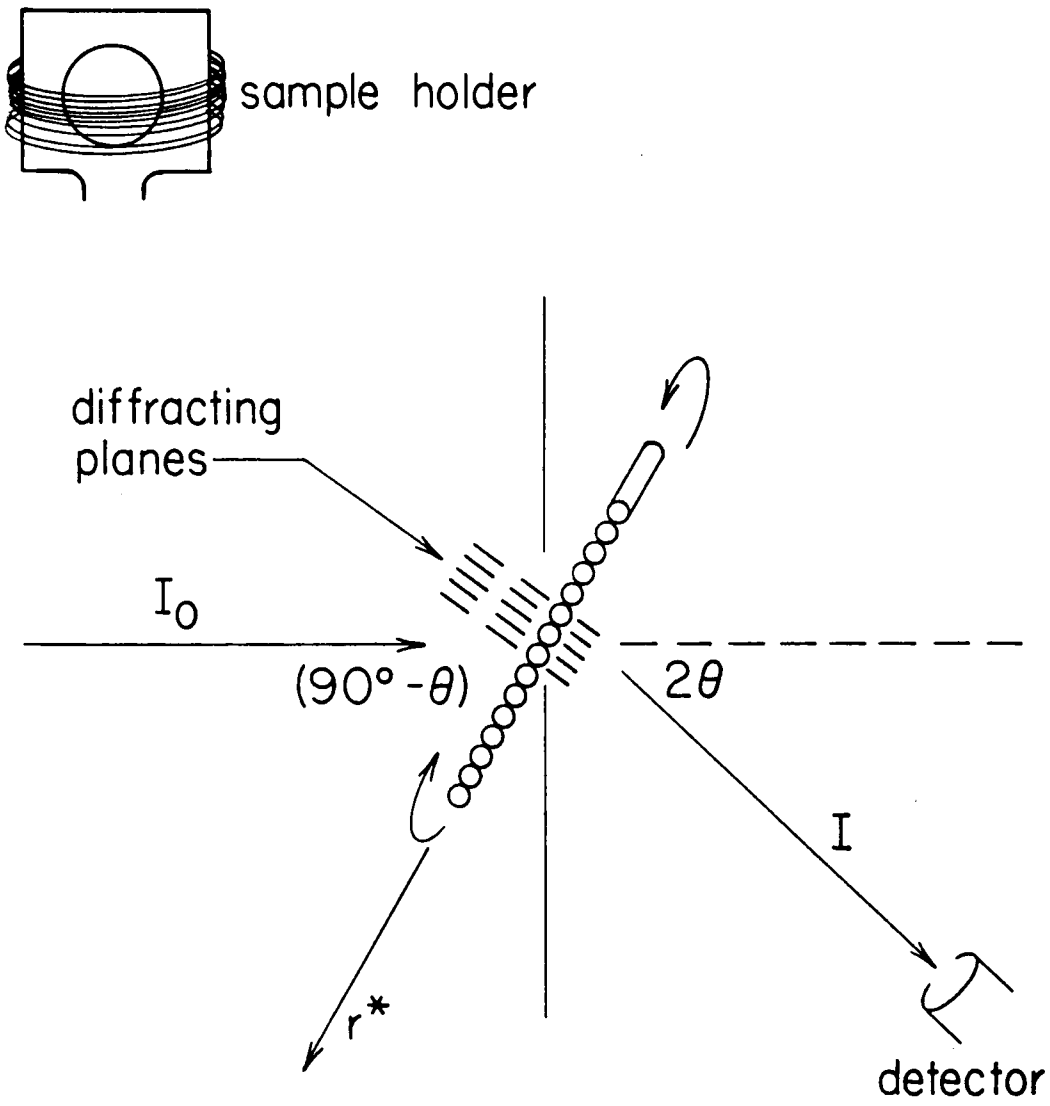

Figure 8. Experimental Arrangement for Orientation Determination of Spun Fibers.

B. ANALYTICAL PROCEDURES

Crystalline Orientation Functions

The orientations of the crystallographic axes, a, b, and c, are conveniently expressed using the Hermans orientation function, as generalized by Stein:

$$f_c = (3\,\overline{\cos^2\phi_c} - 1)/2$$

where ϕ is the angle the c-axis makes with the fiber axis, and the bar over the $\cos^2\phi_c$ indicates that an average is to be taken over all crystals. A value of f_c =1.0 shows the c axes parallel to the fiber axis, and f_c = 0 when the c axes are distributed in a random fashon.

If ϕ_{hkl} is the angle the vector normal to the hkl plane makes with the fiber axis and cylindrical symmetry is assummed, the average value of $\cos^2\phi_{hkl}$ is given by the integral

$$\overline{\cos^2\phi_{hkl}} = \frac{\int I(hkl)\,\cos^2\phi\,\sin\phi\,d\phi}{\int I(hkl)\,\sin\phi\,d\phi}$$

If the (hkl) plane is perpendicular to the C axis, then $\phi_{hkl} = \phi_c$. Using the diffractometer geometry described in the previous section, the diffracted intensity, I(hkl), can be measured directly as a function of ϕ, and the integration can be carried out immediately. When intensity data is obtained from a pinhole pattern, the geometry of Figure 9 applies. In this case $\cos\phi = \cos\Theta\,\cos\alpha$ and

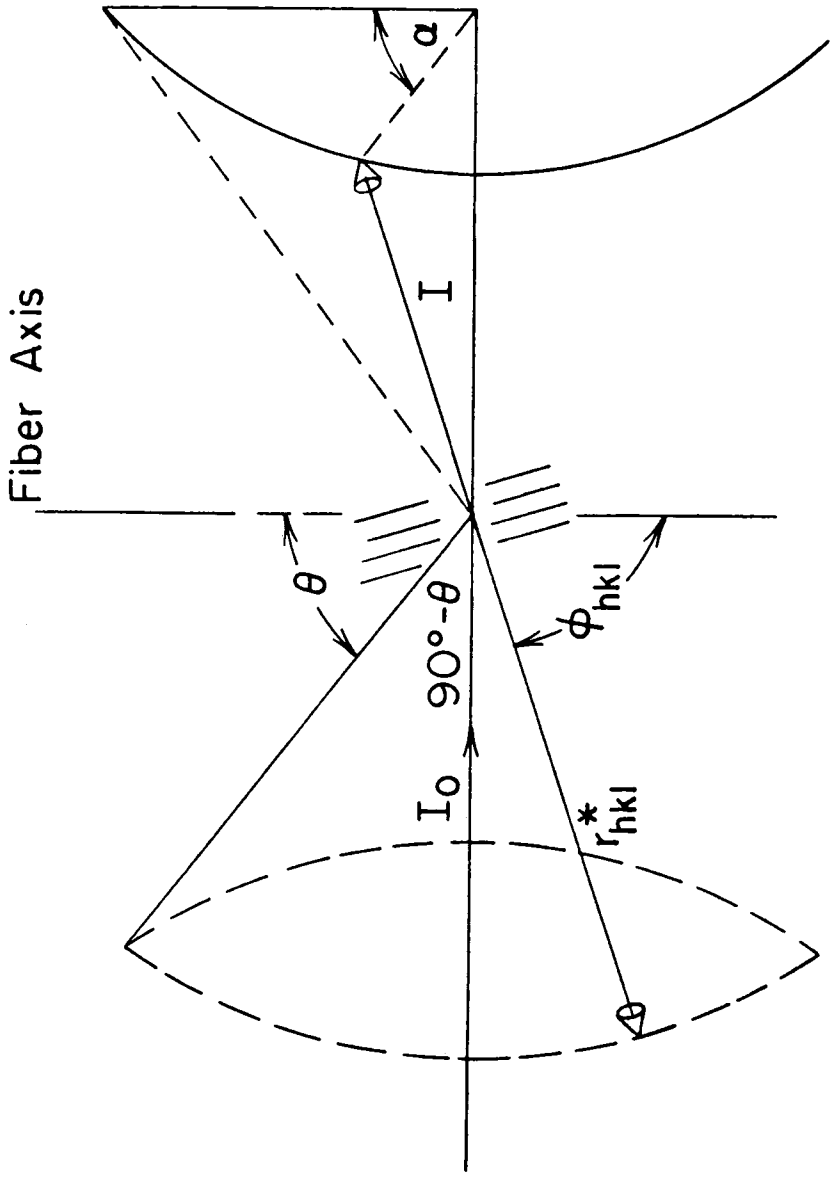

Figure 9. Geometry of a Pinhole Pattern.

$$\overline{\cos^2\phi_{hkl}} = \cos^2\Theta \frac{\int I(hkl)\cos^2\alpha \sin\alpha \, d\alpha}{\int I(hkl)\sin\alpha \, d\alpha}$$

Since the diffraction pattern possesses fourfold symmetry, it is sufficient to perform the integration over one quadrant. The error introduced by integrating from $\alpha = 0°$ to $90°$ was considered to be within experimental uncertainty.

The b crystallographic axis is normal to the 040 planes, therefore $\overline{\cos^2}_b = \overline{\cos^2}_{040}$ may be obtained immediately from measurement of the 040 reflection. However, no reflections having the c axis as their normal are present in the pattern of monoclinic polypropylene. An expression has been derived by Wilchinsky (56) for c-axis orientation in polypropylene film. If ϕ_1 and ϕ_2 are the angles, the normals to two planes containing the c axis make with the fiber axis

$$\overline{\cos^2\phi_c} = 1 - \frac{(1 - 2\sin^2\phi_2)(\overline{\cos^2\phi_1}) - (1 - 2\sin^2\phi_1)\overline{\cos^2\phi_2}}{\sin^2\phi_1 - \sin^2\phi_2}$$

where ϕ_1 and ϕ_2 are the angles the normals to the two planes make with the b axis. The 110 and 040 planes give the most intense Debye rings; using these reflections

$$\overline{\cos\phi_c} = 1 - 0.901\ \overline{\cos^2\phi}_{040} - 1.099\ \overline{\cos^2\phi}_{110} .$$

If a hypothetical axis, a', is defined normal to both the b and c axes of the monoclinic unit cell, its orientation is given by the relationship

$$f_b + f_c + f_{a'} = 0 \ .$$

In a specimen showing the bimodal orientation diffraction pattern shown in Figure 10 the Hermans function as directly obtained from the fiber pattern does not provide sufficient description of crystalline chain axis orientation. An increase in either the number of chains in the secondary population or an increase in their alignment perpendicular to the fiber axis will produce a decrease in f_c, which may compensate for an increase in number or alignment of the primary chains. The compensatory effect makes the analysis of the results in terms of a morphological model difficult.

An attempt to characterize the morphology of biaxially textured samples, therefore, requires a separation of primary and secondary populations. Samuels (40) has used an aximuthal scan of the 110 reflection in order to make this separation. He assumes

1. that each of the two peaks symmetrical about the meridian contributes equally to the intensity at the meridian,
2. the intensity at $\phi = (15°)$ is due to only one of these peaks, and
3. the intensity contribution of the secondary component falls to 0 at $\phi = (56°)$.

The 110 intensity distribution in our samples range from uniform (random orientation) to two distinct peaks with no appreciable intensity between (shown in Figure 11). Samuels' separation was not adequate for the purpose of describing our particular morphology since

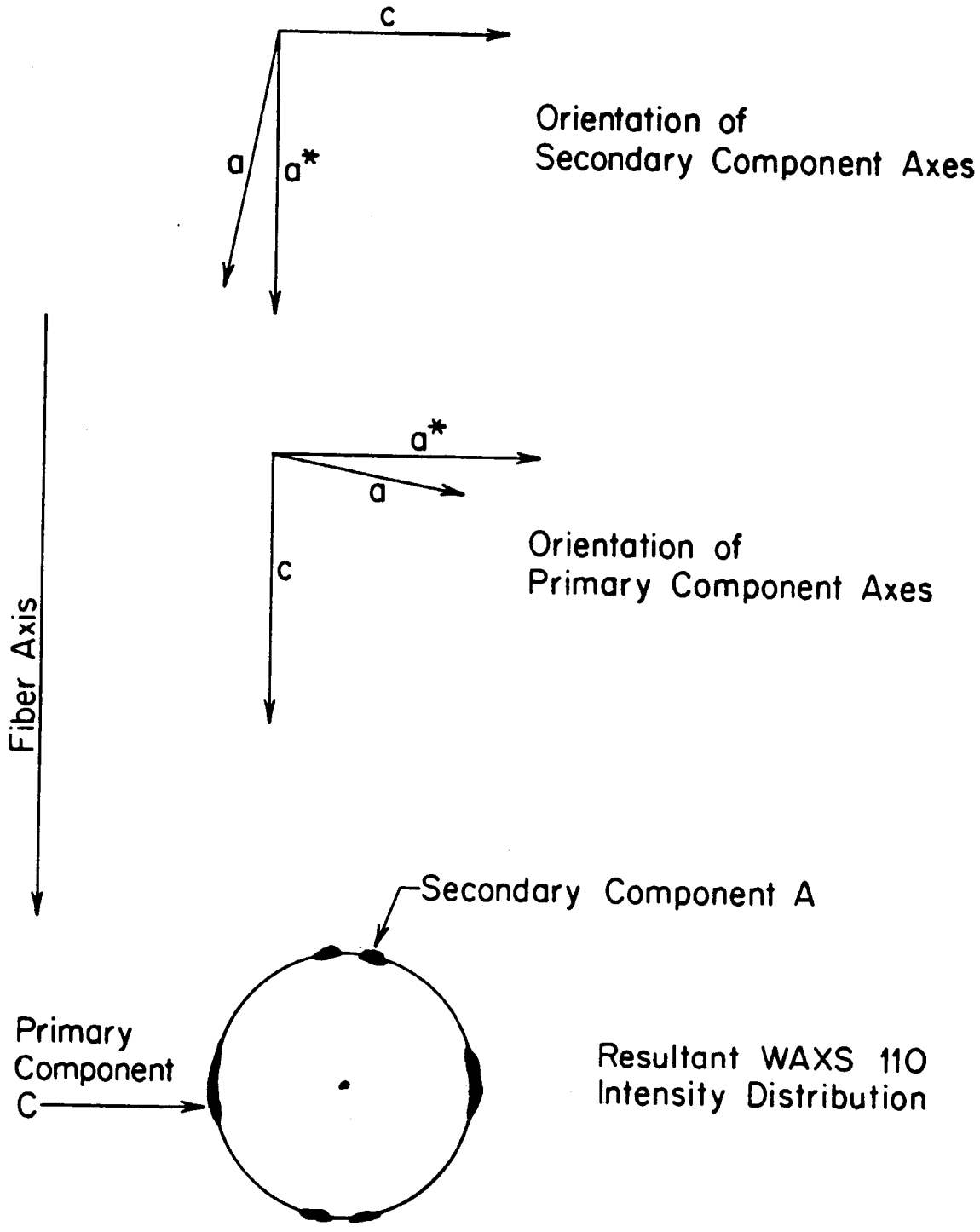

Figure 10. Bimodal Orientation and Resultant Intensity.

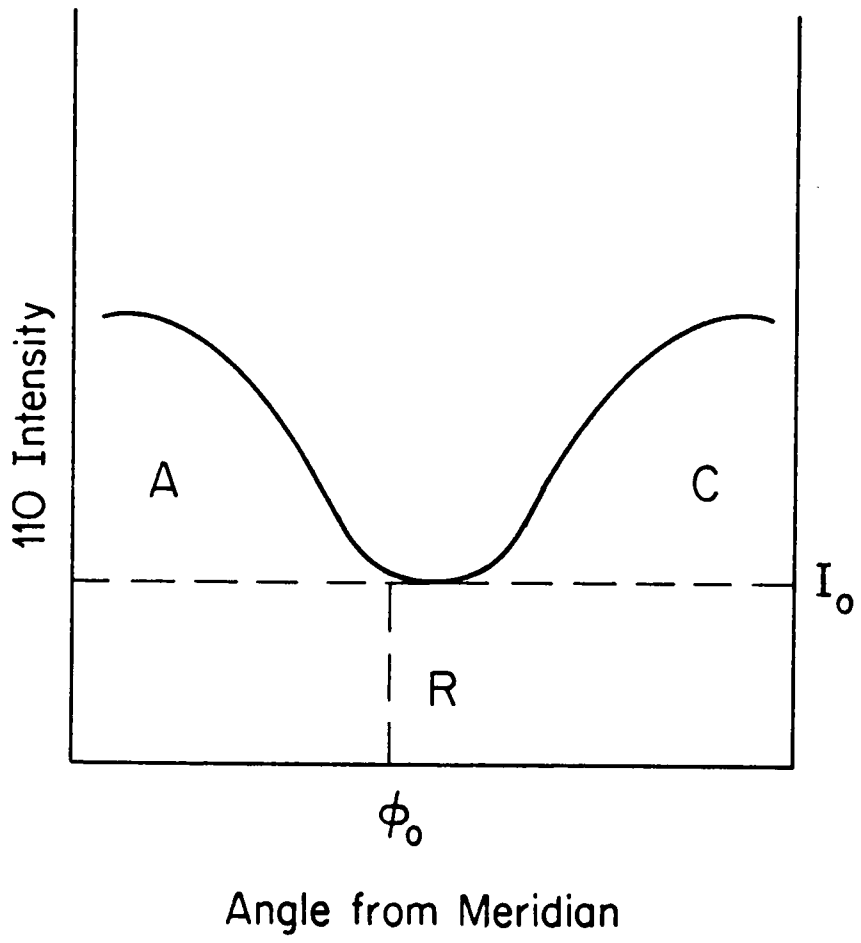

Figure 11. Separation of Primary (C-Axis Oriented), Secondary (A-Axis Oriented), and Random Components.

1. In a spherulitic sample showing completely random orientation assumption (3) gave a wholly artificial separation and orientation of each component, and
2. In a sample with a narrow intensity distribution at the meridian assumption (1) is invalid.

We made an arbitrary separation of three components as illustrated in Figure 11. It was assumed that such an intensity distribution could be represented as the sum of contributions from three continuous distributions of plane normals:

R = random, contributing intensity of area R;C and A--showing distribution of orientations and contributing intensities of areas C and A.

The fractional population and orientation function f_c of component A was calculated from the intensity distribution shown in Figure 11 by the equations

$$pop_A = \frac{\int_o^{\phi_o} (I - I_o)\sin\phi d\phi}{\int_0^{90} I \sin\phi d\phi}$$

$$\overline{(\cos^2\phi_c)}_A = \frac{\int_o^{\phi_o} (I - I_o)\cos^2\phi \sin\phi d\phi}{\int_o^{\phi_o} (I - I_o)\sin\phi d\phi}$$

$$= \frac{1}{pop_A} \frac{\int_0^{\phi} (I - I_o)\cos^2\phi d\phi}{\int_0^{90°} I \sin\phi d\phi}$$

$$(f_c)_A = [3\overline{(\cos \phi c)}_A - 1]/2$$

In a similar manner the population and distribution of the C component was determined. The two advantages of this separation method are (a) no assumptions except continuity need be made about the intensity distribution of either oriented component, and (b) in either unoriented or highly oriented samples inappropriate components disappear.

However when tails of the two oriented distributions C and A overlap, as in slight orientation, intensity in the tails is considered to come from R material. This gives high estimates of the contribution from random chains and high orientation functions for C and A components. Since the maximum of the intensity maximum produced by the A component is contained within the region of integration, the breadth of the distribution of the A component chains about the fiber axis is not measured.

Determination of Crystalline Fraction

The crystalline fraction of the as-spun filaments was calculated from their density by the following equation:

$$X = \frac{V_o^{am} - V}{V_o^{am} - V_o^{x}}$$

where V is measured specific volume, V_o^x is the specific volume of crystalline polypropylene and V_o^{am} is the specific volume of amorphous polypropylene. The latter two quantities must be evaluated at the temperature of the density gradient column. The following expressions were used:

$$V_o^c = 1.059 + (4.25 \times 10^{-4})T$$

$$V_o^{am} = 1.134 + (9.28 \times 10^{-4})T \quad .$$

Crystalline fraction on the spinline was calculated from x-ray diffraction patterns, using the 040 Debye ring. Since b-axis orientation did not vary significantly along the spinning way, 040 peak height at the equator, P, was assumed proportional to the crystalline fraction. Height of the amorphous halo was assumed proportional to the amorphous fraction of the specimen. The ratio P/A was then simply related to the crystalline-amorphous ratio

$$P/A = K \frac{\text{crystalline fraction}}{\text{amorphous fraction}}$$

by the constant

$$K = \frac{\text{height of } A_{100\% \text{ amorphous}}}{\text{height of } P_{100\% \text{ crystalline}}}$$

and is independent of exposure for any given pattern. Measurement of as-spun diffraction pattern(s) and calibration of the degree of crystallinity by using the density crystallinity values yielded the

value of K. Correction was made for air-scattering, using a standard pattern, and background. Measurements are illustrated in Figure 12.

Orientation of Amorphous Regions

The orientation of amorphous regions may be calculated from birefringence data. According to Stein (48), neglecting form birefringence,

$$\Delta n^{tot} = \Delta n^{x} + \Delta n^{am}$$

$$= f_c^{x} X \, \Delta n_i^{x} + f_c^{am}(1 - X) \, \Delta n_i^{am}$$

where Δn_i^{x} and Δn_i^{am} are the intrinsic birefringence of crystalline and amorphous components. Using Samuels' (56) values for intrinsic birefringence with our birefringence measurements, Δn_{tot}, crystalline orientation, f_c^{x}, and crystalline fraction $\overline{X}^{x}$ the orientation of molecular chains in the amorphous region is given by

$$f_c^{am} = \frac{\Delta n^{tot} - f_c^{x} X \, \Delta n_i^{x}}{(1 - X) \, \Delta n_i^{am}}$$

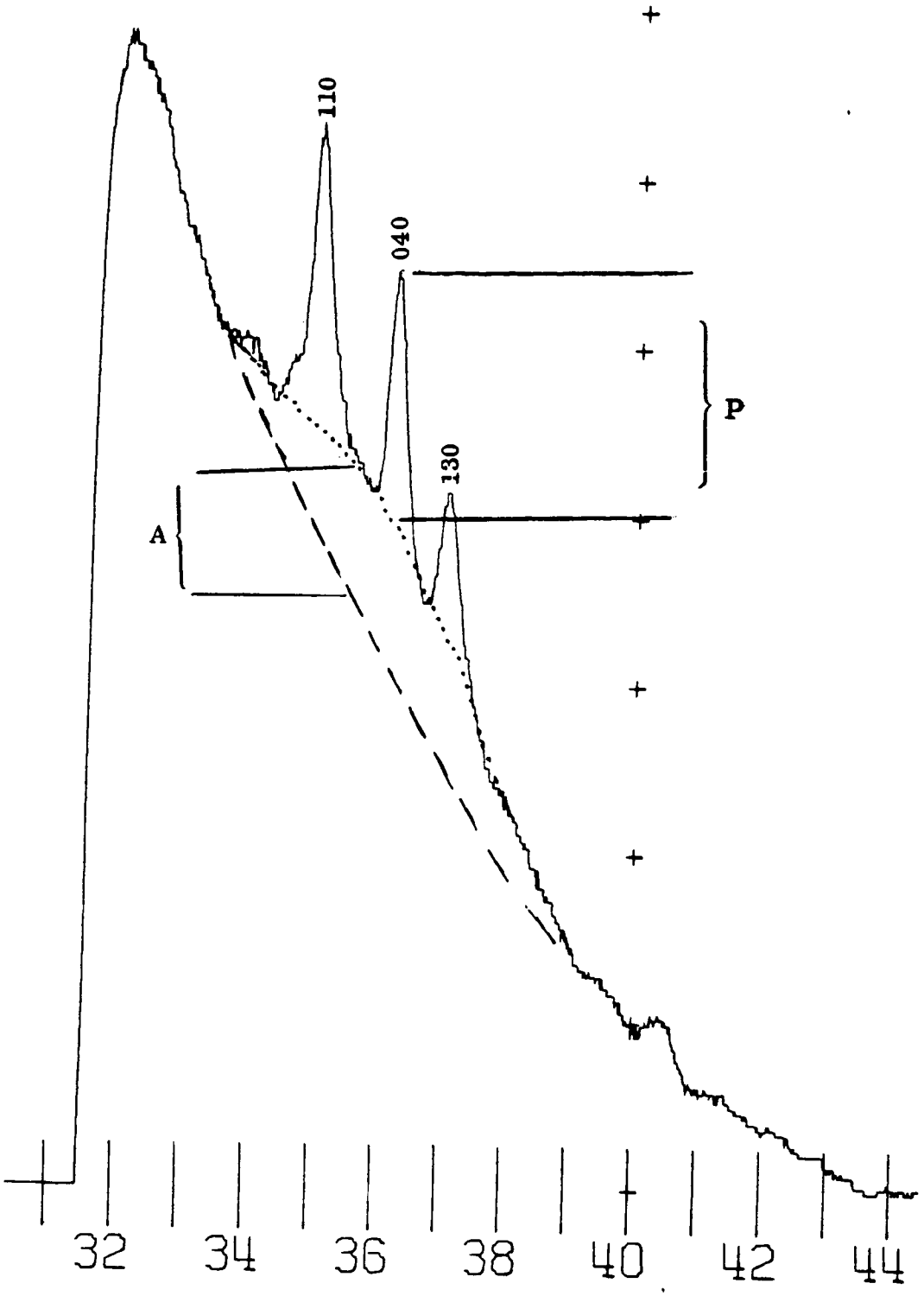

Figure 12. Measurement of Crystalline Fraction.

CHAPTER IV

RESULTS AND DISCUSSION

A. THE AS-SPUN FILAMENTS

Crystalline Fraction

Determinations of crystalline fraction, obtained from density measurements of the as-spun filaments are presented in Table 1. Little variation in crystalline fraction is seen; values range from 0.520 to 0.594. Our data shows little evidence that a significant trend exists with any of the spinning variables investigated.

Crystalline Orientation and Morphology

WAXS and SAXS patterns taken of filaments spun at varying take-up velocities from a polymer melt at temperatures 260°C and 230°C are shown in Figure 13. A nearly uniform distribution of azimuthal intensity is noted in the Debye rings of patterns from the filament spun at a melt temperature 260° and take-up velocity of 50 meters per minute. On the patterns from filaments spun at higher take-up speeds or lower melt temperatures, distinct azimuthal maxima are observed, indicating preferred orientation of the diffracting planes.

Using the techniques described in Chapter III, quantitative measurements of crystalline orientation were made and are plotted in Figure 14 as a function of take-up velocity. They are seen to be qualitatively consistent with the work of Kitao (32) as each melt temperature is treated separately.

Table 1

Crystalline Fraction of As-Spun Filaments

Melt Temperature (°C)	Take-Up Velocity (m/min)	Crystalline Fraction
260	50	0.545
	100	0.525
	300	0.555
	500	0.520
	550	0.520
230	50	0.557
	100	0.583
	200	0.562
	300	0.542
	500	0.546
	550	0.552
200	50	0.545
	100	0.536
	200	0.545
	300	0.578
	550	0.594

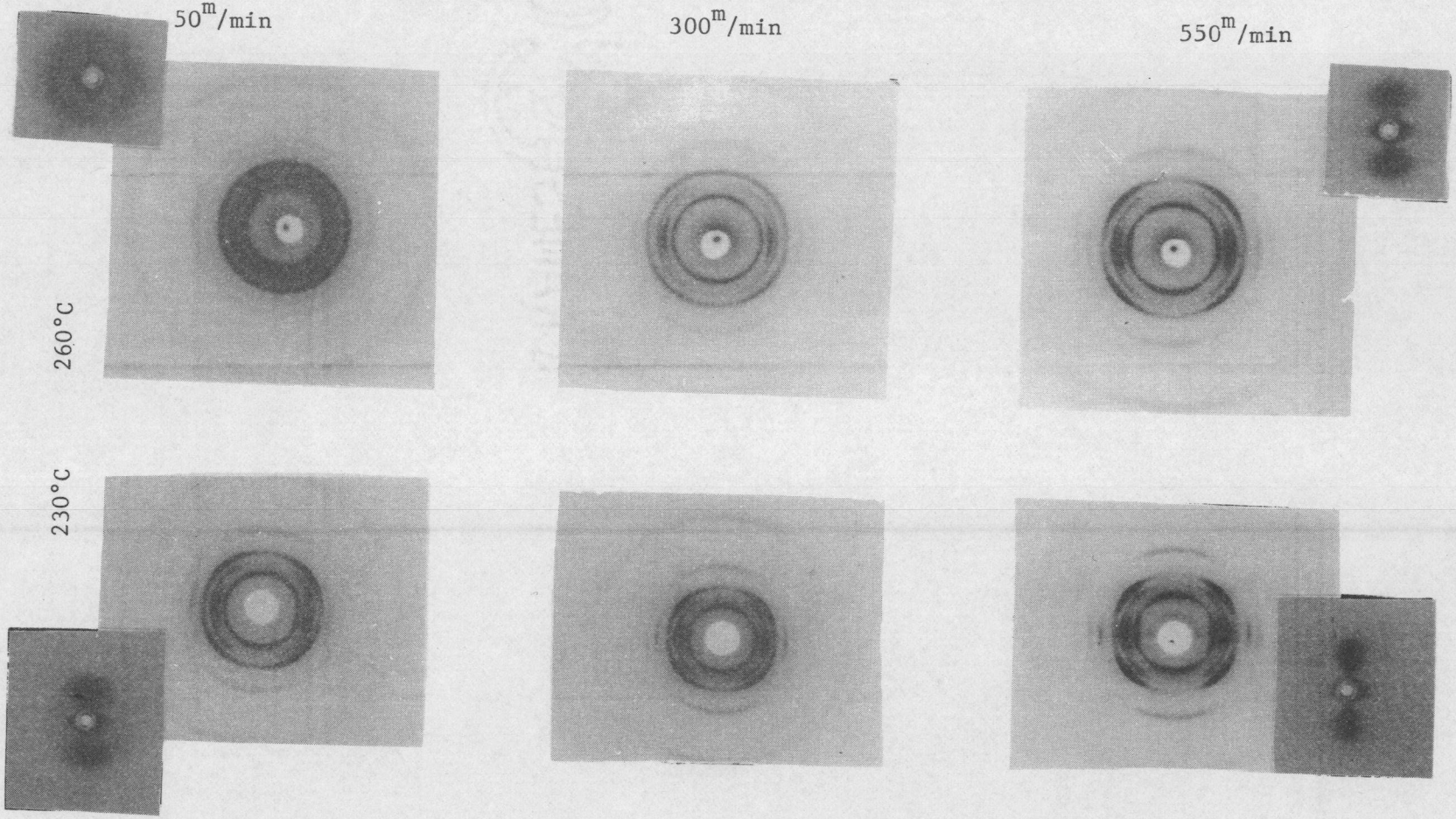

Figure 13. WAXS and SAXS Patterns of Melt-Spun PP Filaments.

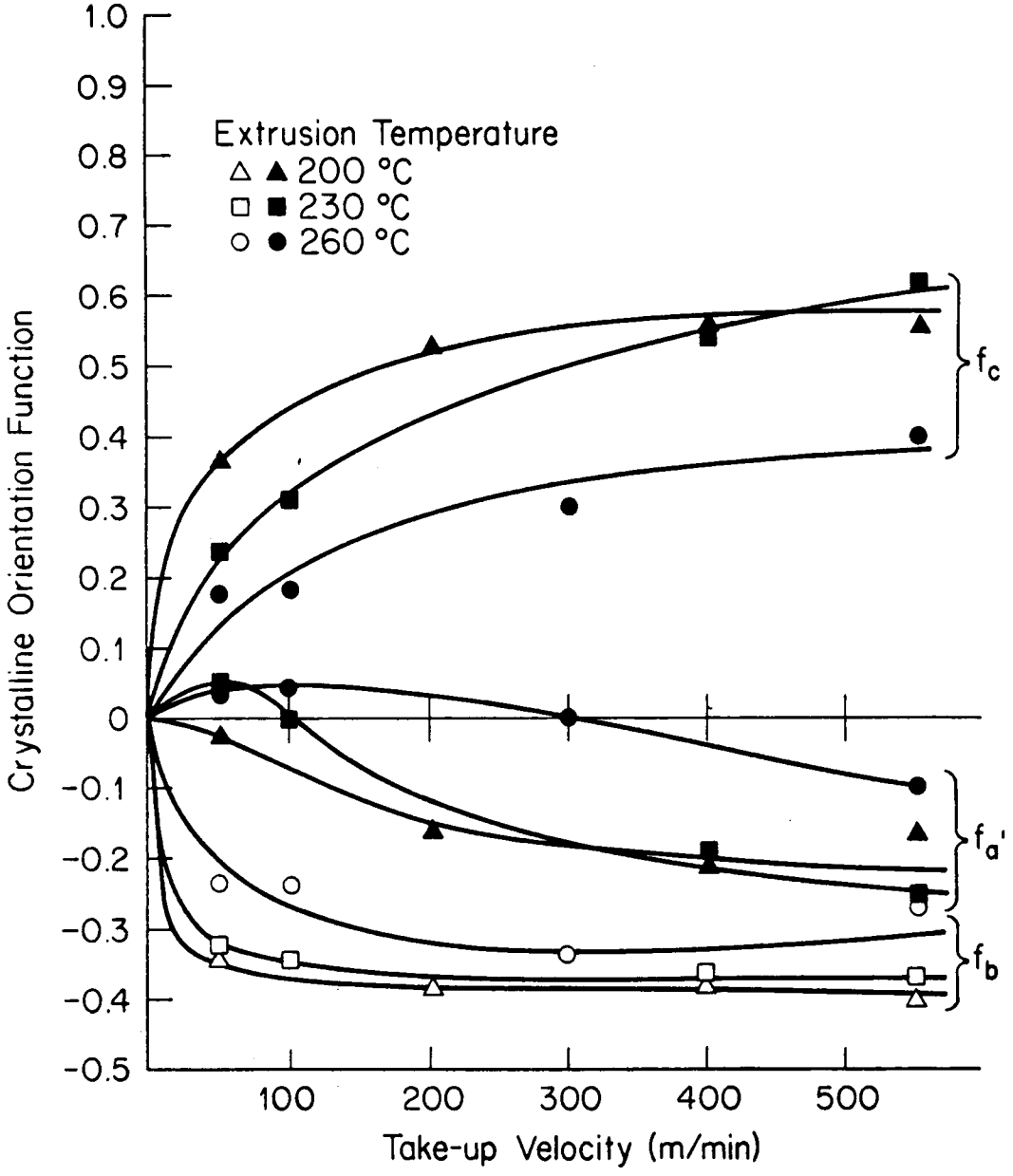

Figure 14. Crystalline Orientation Functions as a Function of Take-Up Velocity for Polypropylene Fibers Spun at Three Melt Temperatures.

When the same data are plotted in Figure 15 versus nominal spinline stress, (filament tension/final fiber diameter) it is seen that our orientation values may be expressed as a function of spinline stress alone. All data points are adequately represented by a single set of curves. The orientation of the b-axes are observed to change rapidly with spinline stress from the zero value of f_b typical of a random distribution, to a limiting orientation of $f_b = -0.4$, indicating the b axes are nearly perpendicular to the fiber axis. Only minor change is observed at stresses higher than 5×10^{-6} dynes per centimeter squared. The average orientation of the c, or chain axis, more gradually rises to its limiting value of 0.6, indicating a distribution of chains tending to parallel the fiber axis. The behavior of the a' axis of the pseudo-orthorhombic unit cell is more complex; at low stresses leaning on the average toward the fiber axis, then, as spinline stress is increased, becoming, on the average, tilted toward a perpendicular orientation.

These results are strikingly similar to those observed in the case of polyethylene (14, 15). However, as discussed in Chapter III, an estimate of the contributions of the primary and secondary populations to the overall crystalline orientation must be made before further discussion of morphology. The arbitrary separation of primary and secondary components described was used, and estimates of the relative amounts of material in the A, C, and R populations were made. These are plotted in Figure 16. It is noted that with increasing stress, the relative contribution of the C population to the observed orientation becomes much greater. Using the relationship

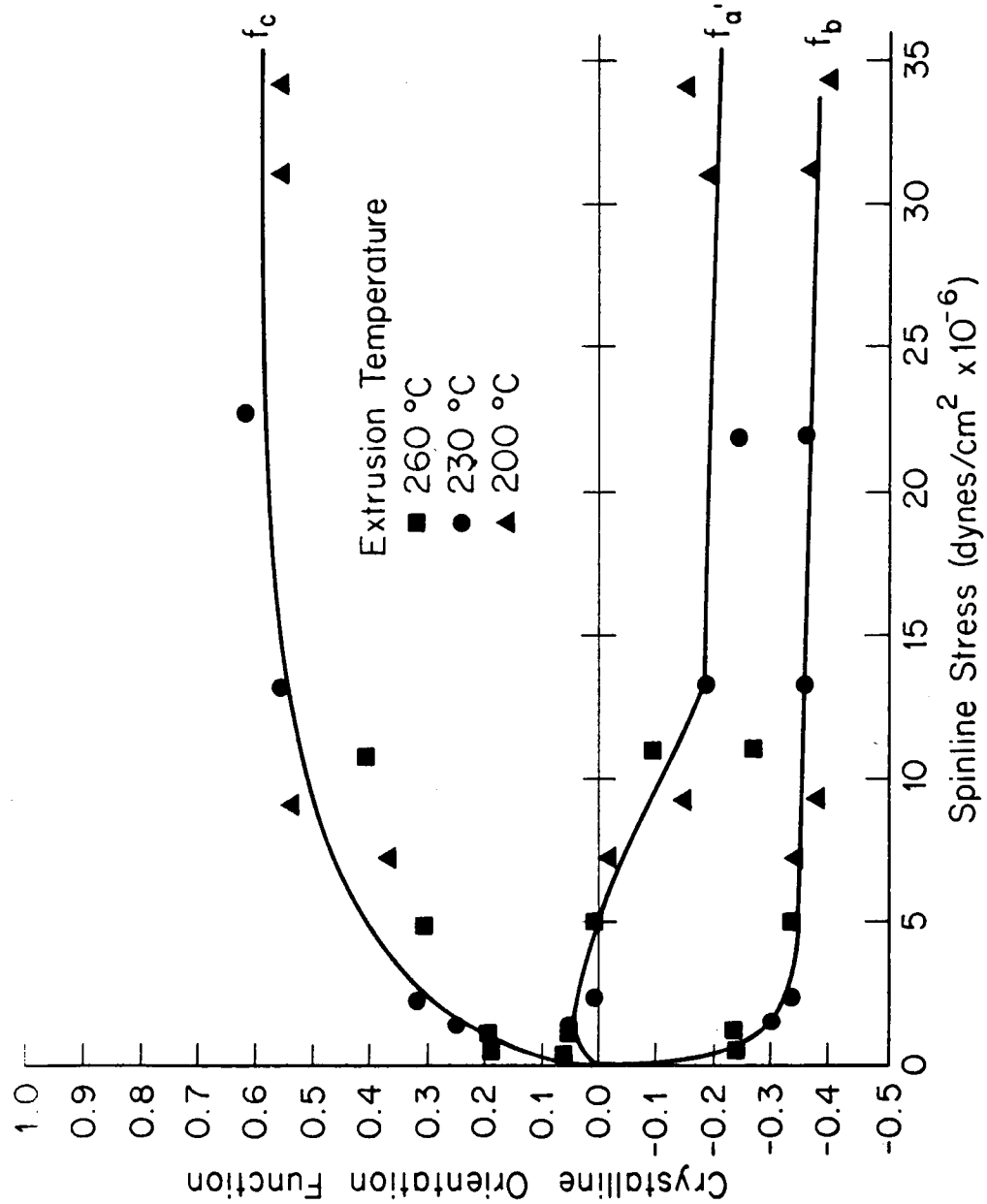

Figure 15. Crystalline Orientation of Melt-Spun Fibers as a Function of Spinline Stress.

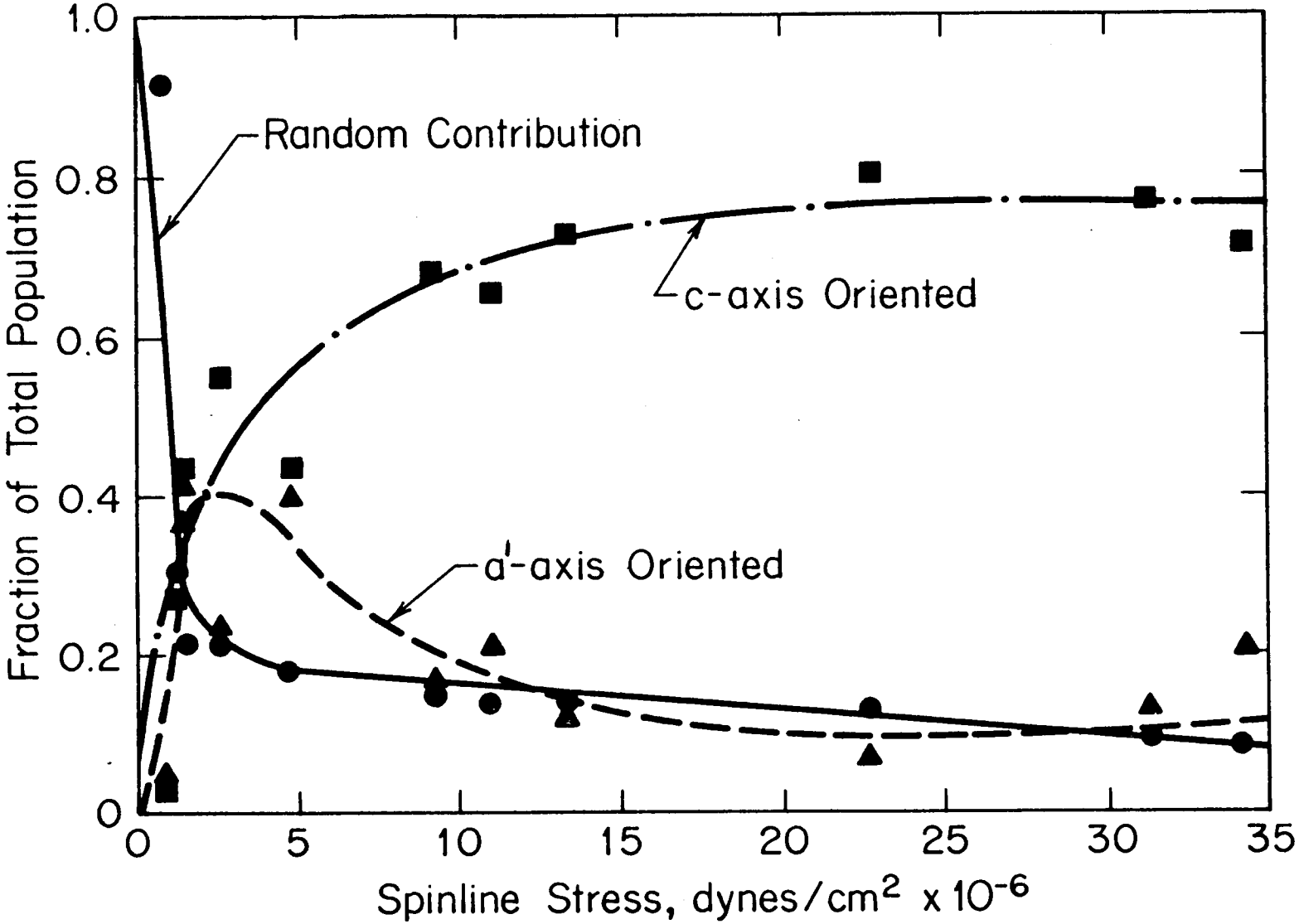

Figure 16. Relative Fractions of Primary (C) and Secondary (A) Components Versus Spinline Stress.

$$\overline{\cos^2\phi}_{110} = \frac{\overline{\cos^2\phi}_R[\text{pop R}] + \overline{\cos^2\phi}_C[\text{pop C}]}{[\text{pop R} + \text{pop C}]}$$

orientation functions were calculated neglecting the A component. Results are shown in Figure 17 as a function of spinline stress. It may be seen that as in the case of overall orientation, the c and a' axes orientation develops more slowly than that of the b axis.

The most straightforward interpretation of these data is in terms of the model put forward by Dees and Spruiell for the case of the melt-spun polyethylene. This model has been shown in Figure 4 (page 17). At low stress levels, the structure is considered spherulitic and results from growth from point nuclei. As stress levels increase, row nucleation occurs, and growth occurs radially perpendicular to the fiber axis. As previously discussed in Chapter II, the b-axis of monoclinic polypropylene is generally considered to be tangential to the growth direction; its rapid assumption of a position nearly at right angles to the fiber axis is consistent with growth in this perpendicular plane. The slower alignment of the c and a' axes could, as in polyethylene, be indicative of lamellar irregularities. These irregularities decrease as the stress in the filament during solidification increases.

The high alignment of the b axis relative to the a and c axes is also consistent with the formation of the deformed spherulites, flattened in the direction of stress, previously suggested based on light scattering results (40). It is our view, however, that such shapes will occur only as an intermediate form between true spherulites and a well developed row structure. They form as a result of the shift in

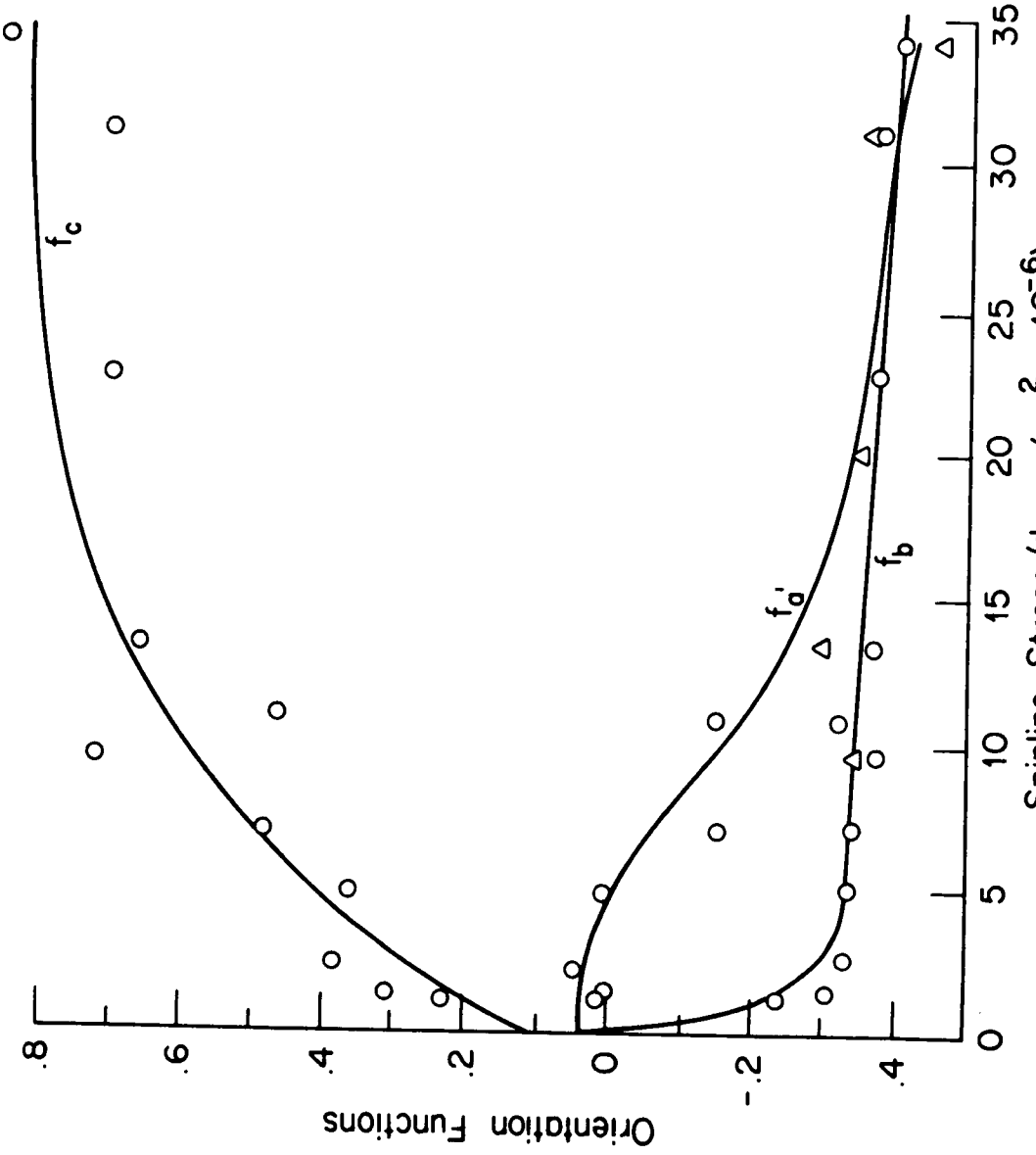

Figure 17. Crystalline Orientation of Melt-Spun Fibers (Neglecting A-Component) as a Function of Spinline Stress.

nucleation and growth conditions toward fibril nuclei and rapid impingement in the direction along the fiber axis, rather than as a result of deformation of a spherical shaped entity.

The development of a row structure at intermediate and high spinline stresses is confirmed by small angle x-ray diffraction, as shown in Figure 13 (page 52). All small angle patterns taken at stress levels above 4×10^6 dynes/cm^2 showed the meridional maxima characteristic of lamellae stacked in the direction of the fiber axis.

This model is indirectly supported by the work of Baranov and Volkov, who found, as discussed in Chapter II, that at low melt-draw ratios, flattened spherulites occurred, but at higher draw-down ratios an "oriented phase" appeared, and as draw-down ratio increased, the spherulites disappeared altogether. Their oriented phase would correspond to the appearance of the row structure.

Orientation of Amorphous Regions

Birefringence data for the as-spun fibers is plotted in Figure 18 against spinline stress, and like the crystalline orientation functions, a single curve is sufficient to represent all data points.

Using the method described in Chapter III, the observed birefringence was separated into contributions from the crystalline and the amorphous regions. The amorphous contribution is plotted with the overall birefirengence in Figure 18.

Mechanical Properties

Typical stress-strain curves are shown in Figure 19 for fibers spun at low and high stress levels. The fiber spun at low stress exhibits

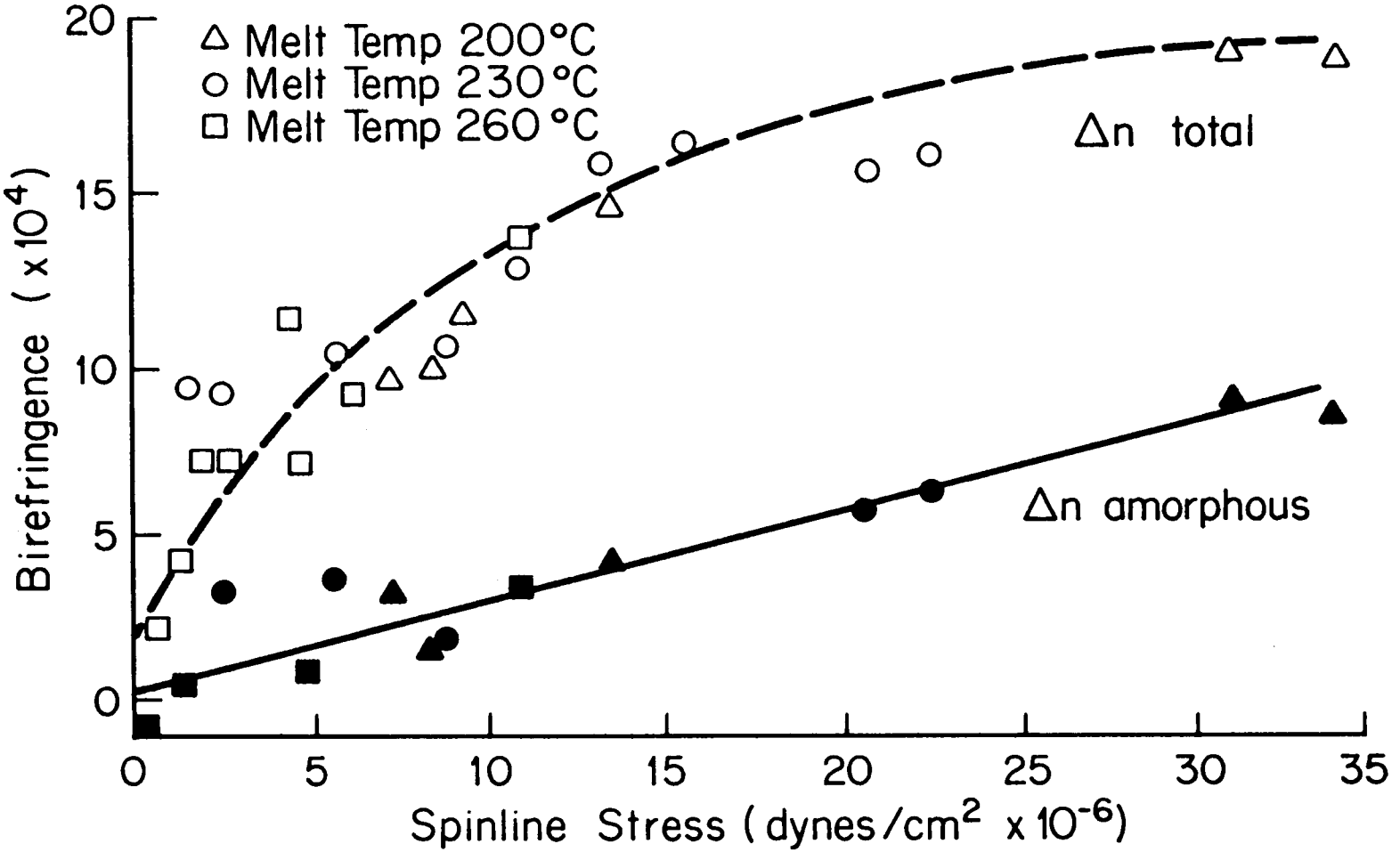

Figure 18. Birefringence of As-Spun Filaments and Contribution Due to Orientation of Amorphous Material as a Function of Spinline Stress.

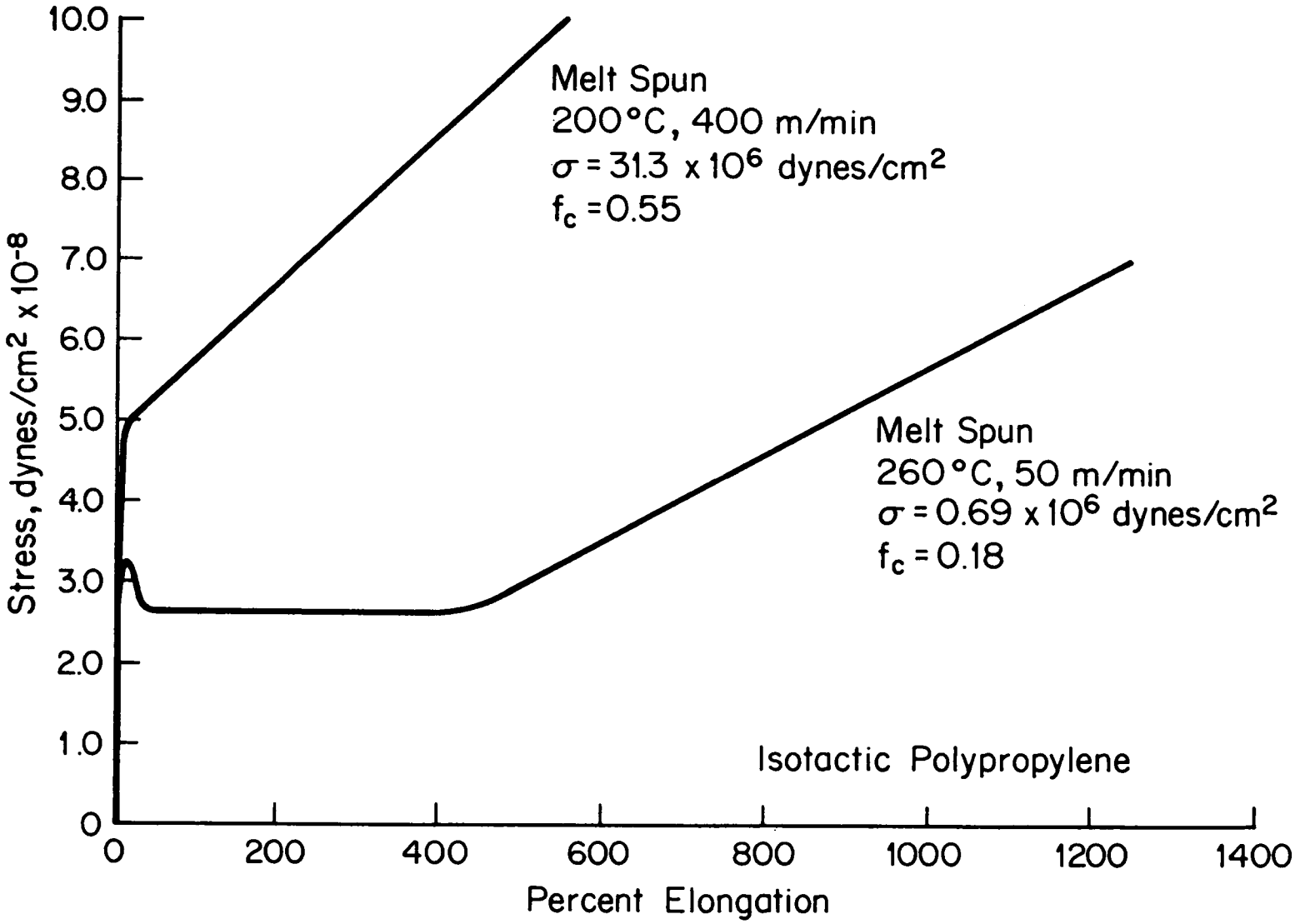

Figure 19. Typical Stress-Strain Curves Obtained from Fibers Spun at Low and High Spinline Stress.

prominent necking and high ultimate strength as measured by elongation to break. The curve shown for the fiber spun at higher-stress is similar to those shown by Sprague (47) for "hard elastic" fibers. Annealing confirms, as shown in Figure 20, that at spinline stress of above 5×10^{-6} dynes/cm^2 our spun fibers show high elastic recovery.

This corresponds to the development of the row structure previously discussed. Indications that changes in mechanical properties might be correlated with the development of crystal morphology led to plotting variables such as tensile strength and percent elongation to break as a function of crystalline orientation function as shown in Figure 21. These correlated to some extent. Tensile strength increased with orientation function; a decrease in elongation to break was seen with increased orientation.

B. ON-LINE STUDIES OF SPINNING

Crystallization Start Temperature

Data obtained as described in Chapter II for a typical spinline is shown in Figure 22. Diffraction patterns indicate the point at which crystalline reflections appear. Associated with that point in all our spinline profiles is a change in the slope of the filament surface temperature curve. This is a result of the release of the enthalpy of crystallization, which, in some cases, leads to an actual hold or plateau in the curve. The temperature at this crystallization point is plotted against spinline stress for different sets of spinning conditions in Figure 23. The low crystallization temperatures observed (T_m is nominally 168°C) presumably show the effect of the high cooling rates

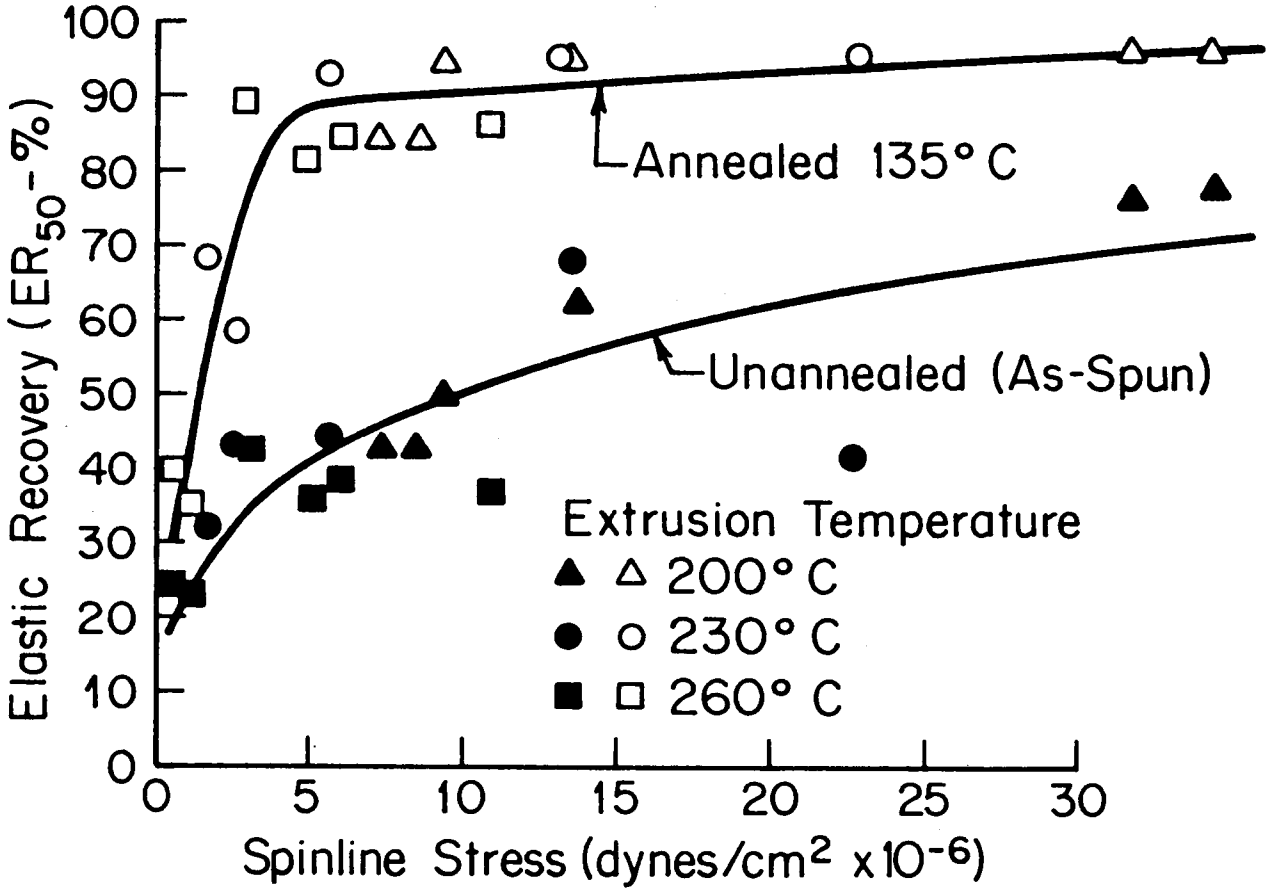

Figure 20. Elastic Recovery of Filaments as a Function of Spinline Stress.

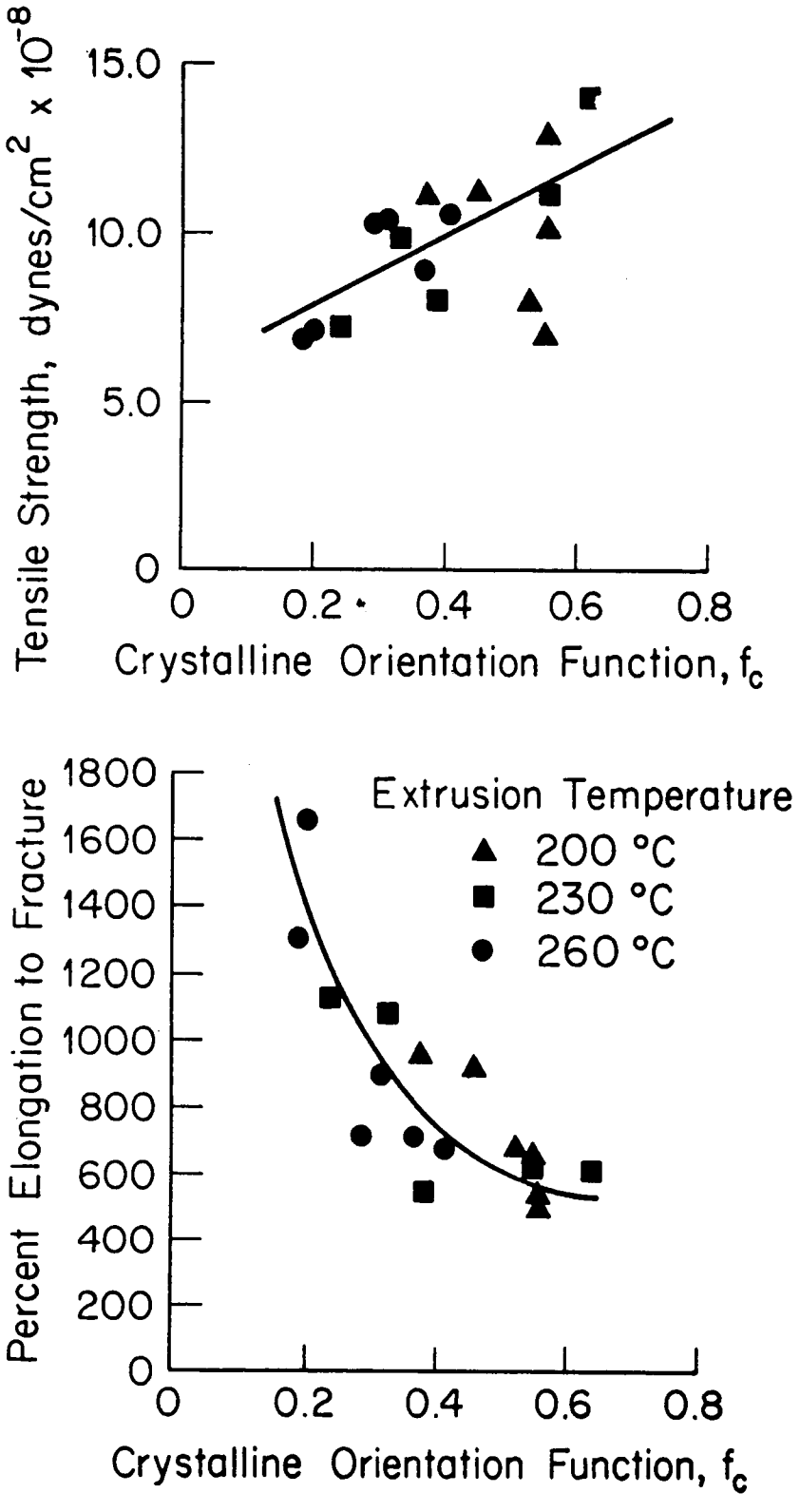

Figure 21. Mechanical Properties of Filaments as a Function of C-Axis Orientation.

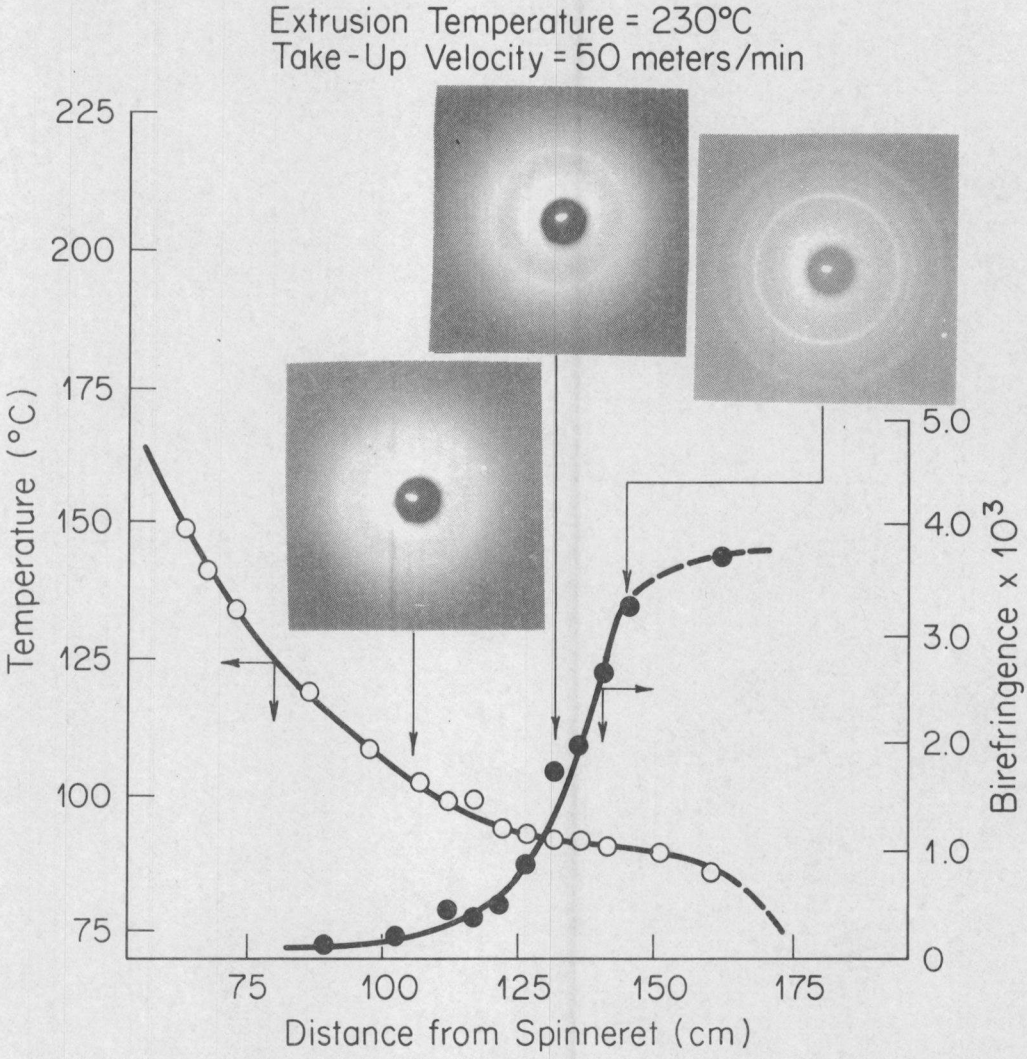

FIGURE 3. On-line WAXS patterns, temperature and birefringence profiles for melt spun H-0660 polypropylene filament.

Figure 22. On-Line WAXS Patterns with Temperature and Birefringence Profiles for Melt-Spun Polypropylene Filament.

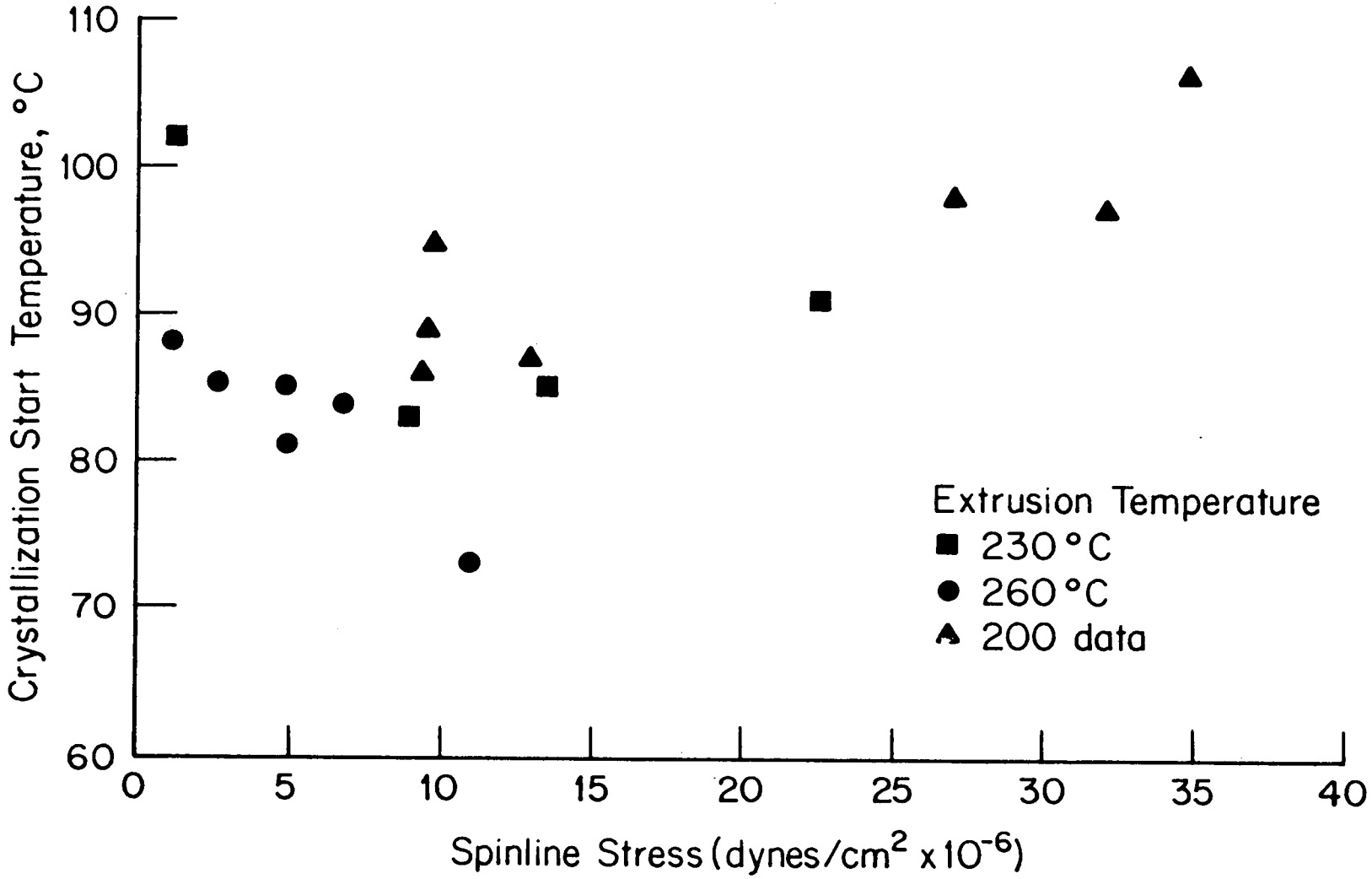

Figure 23. Crystallization Start Temperatures on the Spinline as a Function of Spinline Stress.

encountered on the spinline due to both the large surface-to-volume ratio of the filament and its rapid movement through the cooling medium. An increase in both of these factors is produced with an increase in take-up velocity; relative cooling rate, measured just above the crystallization point can be considered, to a first approximation, a function of take-up velocity alone. This is demonstrated on page 69.

Even at these high cooling rates, however, transformation temperatures measured on the spinline remain in the same range as those obtained in the differential scanning calorimeter at relatively low cooling rates, as can be seen from comparing Table 2 with Figure 23.

Table 2

Transformation Temperatures of Quiescent PP Melts

DSC Cooling Rate (°C/min)	Crystallization Start Temperature (°C)	Crystallization Temperature (°C)
5	123	117
10	120	113
20	117	107
40	111	99

This result apparently follows from greatly enhanced crystallization kinetics due to the applied stress. If this is the case the crystallization start temperature should increase with increased stress at a

given cooling rate. This was checked by comparing the crystallization start temperatures of several spinlines running at the same take-up velocity but different extrusion temperatures. This resulted in similar cooling rates in the temperature range just prior to crystallization temperature, but different take-up stresses (Figure 24).

The results are shown in Figure 25 for three nominal cooling rates. Within our range of spinning conditions the effect of increasing stress is seen to be a raising of the transformation temperature. An empirical fit to our data was obtained by the equation

$$Tx = 90 + \frac{(\sigma)(CR)}{840} - .022\ CR$$

where σ is stress in dynes/cm^2 $\times$ 10^{-6} and CR is cooling rate in °C/sec.

Crystallization Kinetics

Crystallinity levels obtained from on-line WAXS patterns such as those shown in Figure 24 are plotted as a function of spinline residence time in Figure 26. These results should be interpreted in terms of both stress and cooling rates. It is convenient to do this in terms of "continuous cooling transformation" curves used in metallurgy to interpret solid-phase transformations, as discussed by Spruiell and White (48). Such curves are shown schematically in Figure 27. Decreased crystallization start temperatures are observed with increased cooling rate. The effect of stress is to shift the curve toward the y-axis (i.e., to shorten crystallization time). Our data does show such an effect; this is shown in Figure 28.

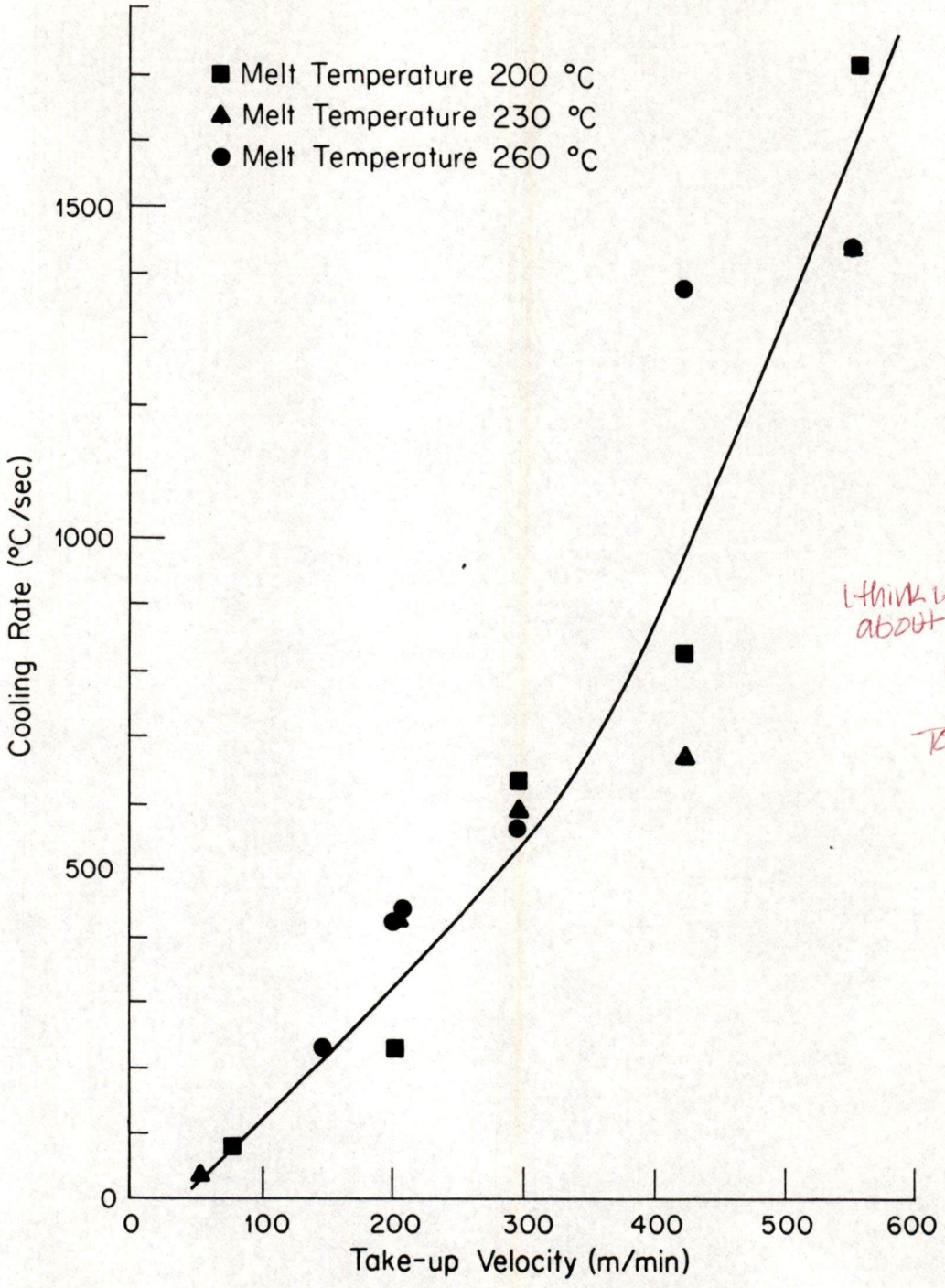

Figure 24. Measured Cooling Rate as a Function of Take-Up Velocity.

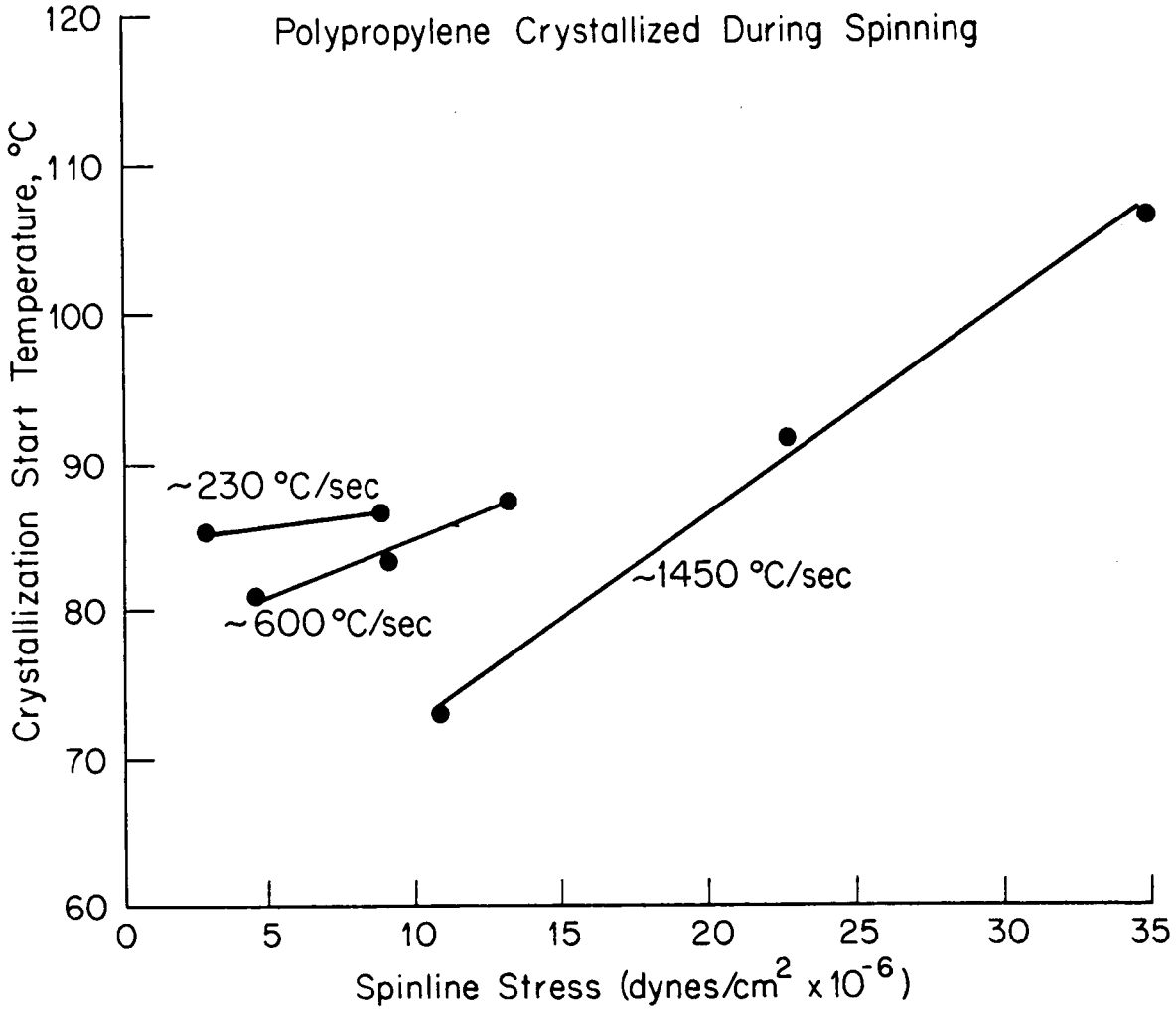

Figure 25. Crystallization Start Temperature Versus Stress at Several Cooling Rates.

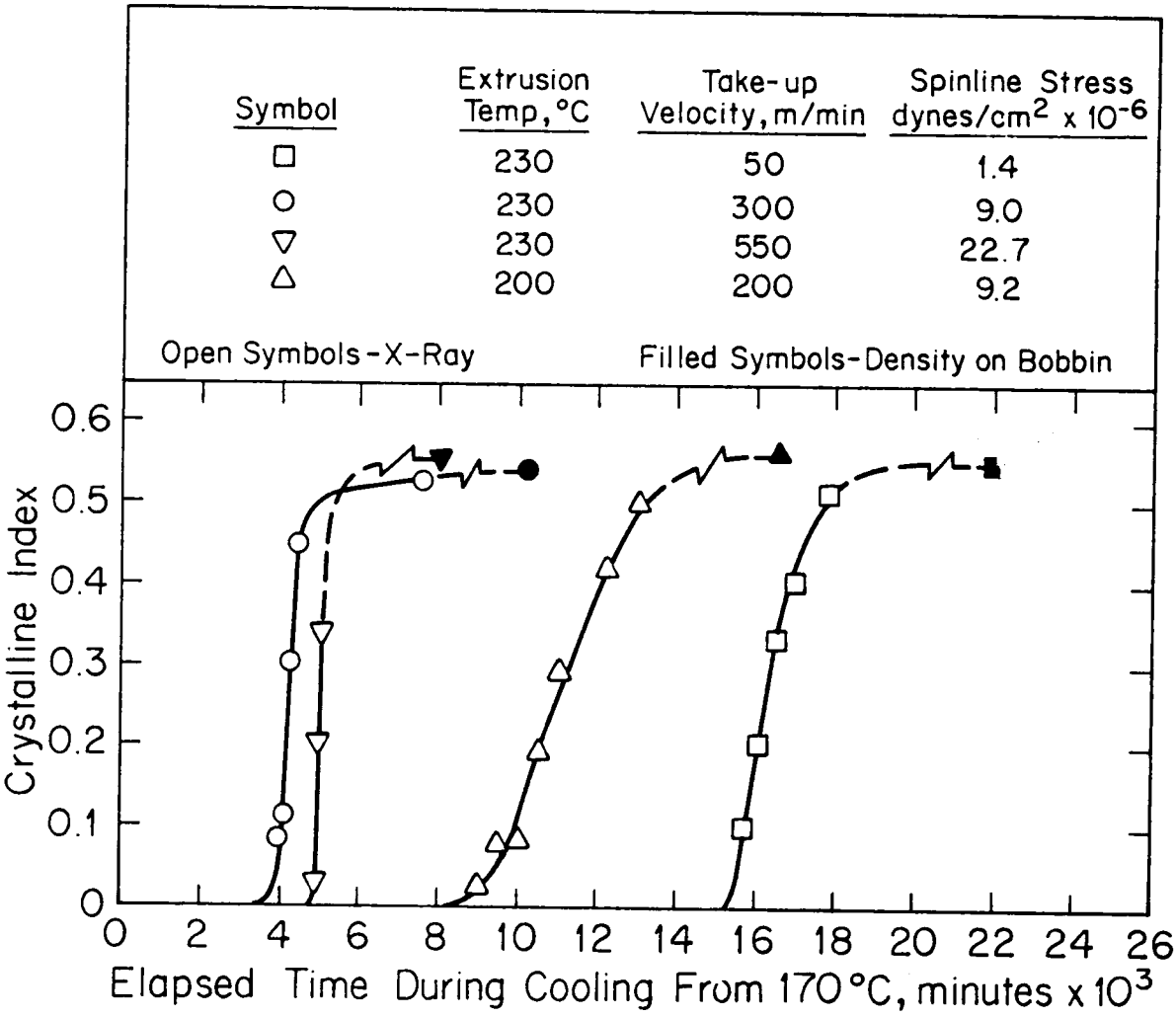

Figure 26. Crystalline Index as a Function of Spinline Residence Time from Analysis of WAXS Patterns.

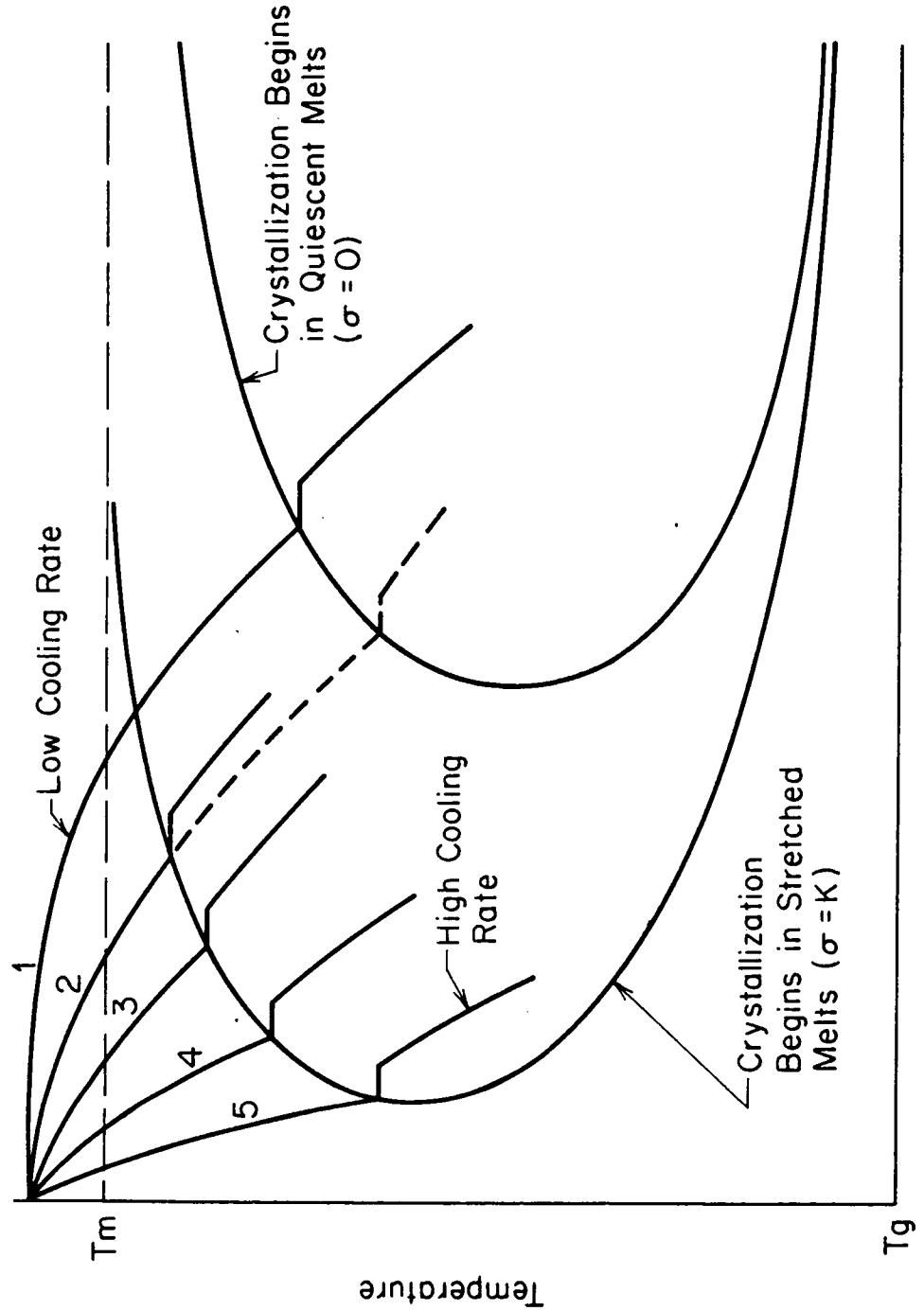

Figure 27. Crystallization Start Temperature as a Function of Cooling Rate for Quiescent and Stressed Melts.

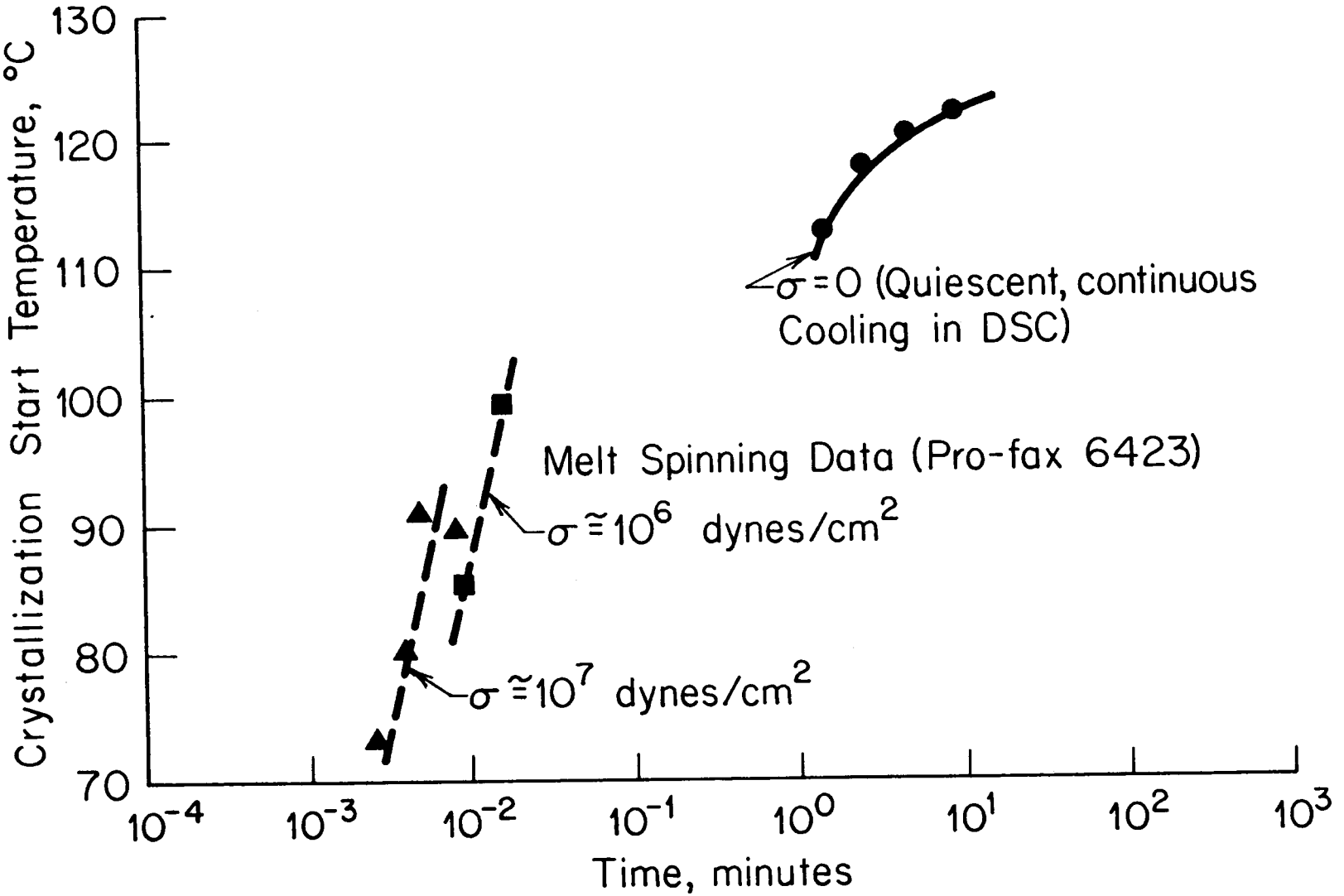

Figure 28. A Comparison of Spinline Crystallization Temperatures with Those Obtained upon Continuous Cooling of Quiescent Melts.

The Development of Overall Orientation

Figure 29 shows a plot of birefringence versus distance from spinneret for fibers spun at two take-up velocities from a 230°C melt and at one corresponding take-up velocity from a 200°C melt. Orientation development is seen to proceed more rapidly at increased stress and with cooling rate (take-up velocity) held constant. As discussed previously the observed birefringence will reflect changes in both amount and orientation of the crystalline and amorphous fiber fractions.

The Development of Crystalline Orientation and Morphology

Figure 30 shows a series of x-ray diffraction patterns taken along a moving spinline (melt temperature 200°, take-up velocity 200 m/min). As Katayama et al. (25) observed, the first 110 reflections to appear are those produced by the C component, the primary population of crystallites containing polymer chains oriented toward the fiber axis. Relative amounts of A and C components as a function of time along this spinline are shown in Figure 31. It may be seen that the increase of the A component fraction contributes to the overall decrease in c-axis orientation with time. Crystalline orientation functions are shown in Figure 32 as a function of spinline residence time. The first crystals to form are seen to possess high c-axis orientation; as crystallization proceeds orientation functions rapidly approach their final values. This is fully consistent with the model proposed by Clark and Spruiell (12), i.e., crystallization proceeding in two stages. In the first stage a row structure of planar lamellae develops from fibril nucleii.

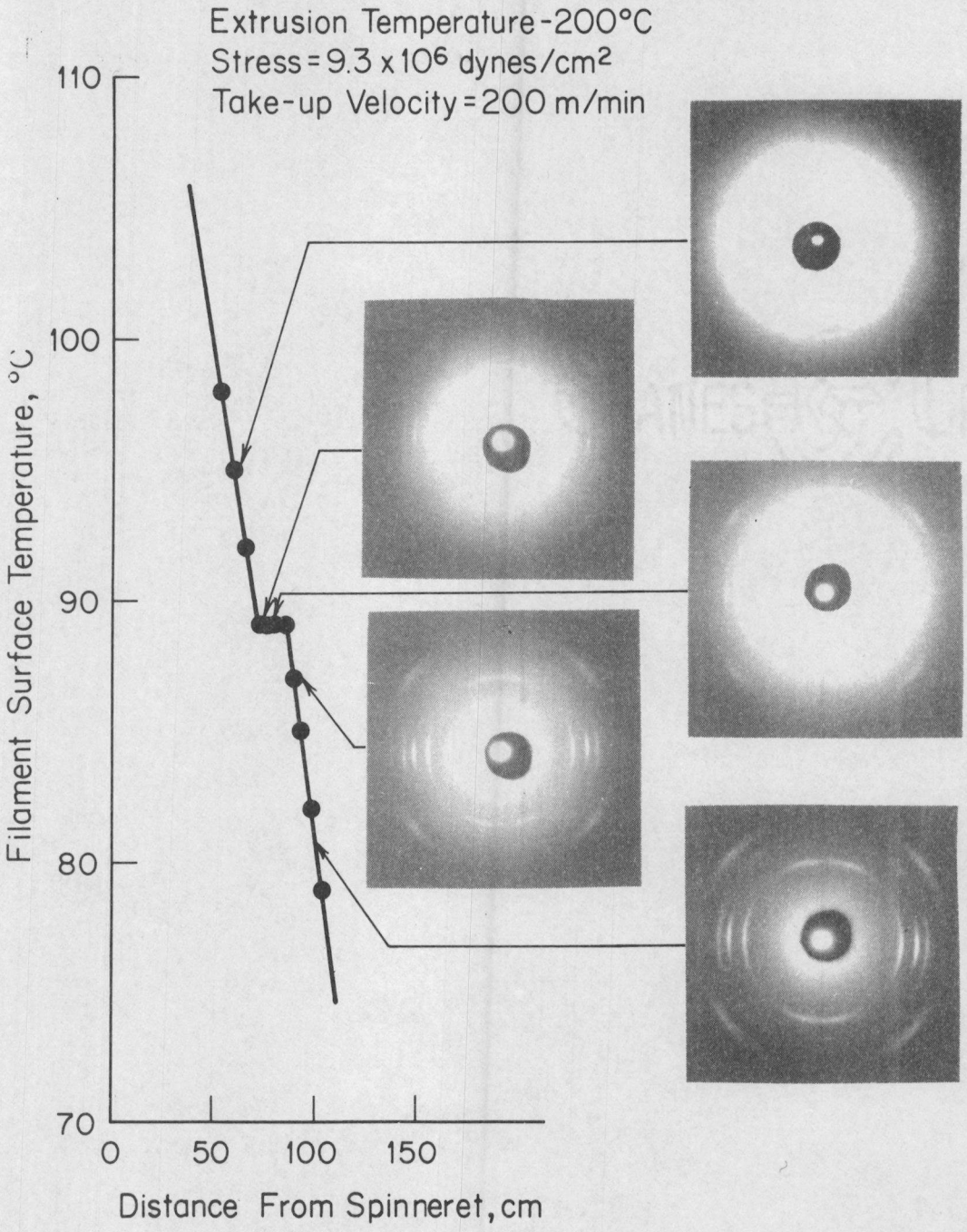

Figure 29. On-Line WAXS and Temperature Profile for Melt-Spun Polypropylene Filament.

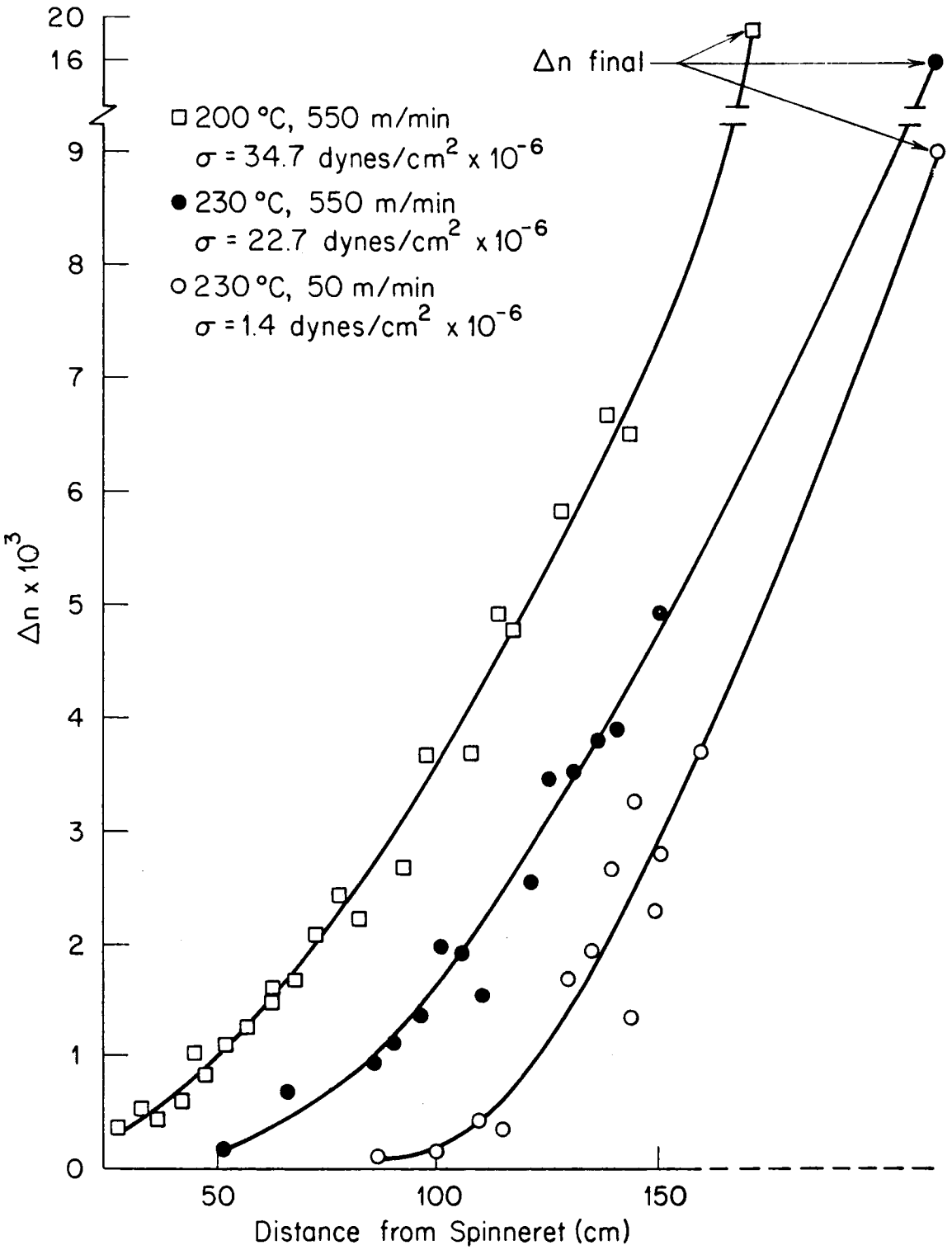

Figure 30. Orientation Development on the Spinline.

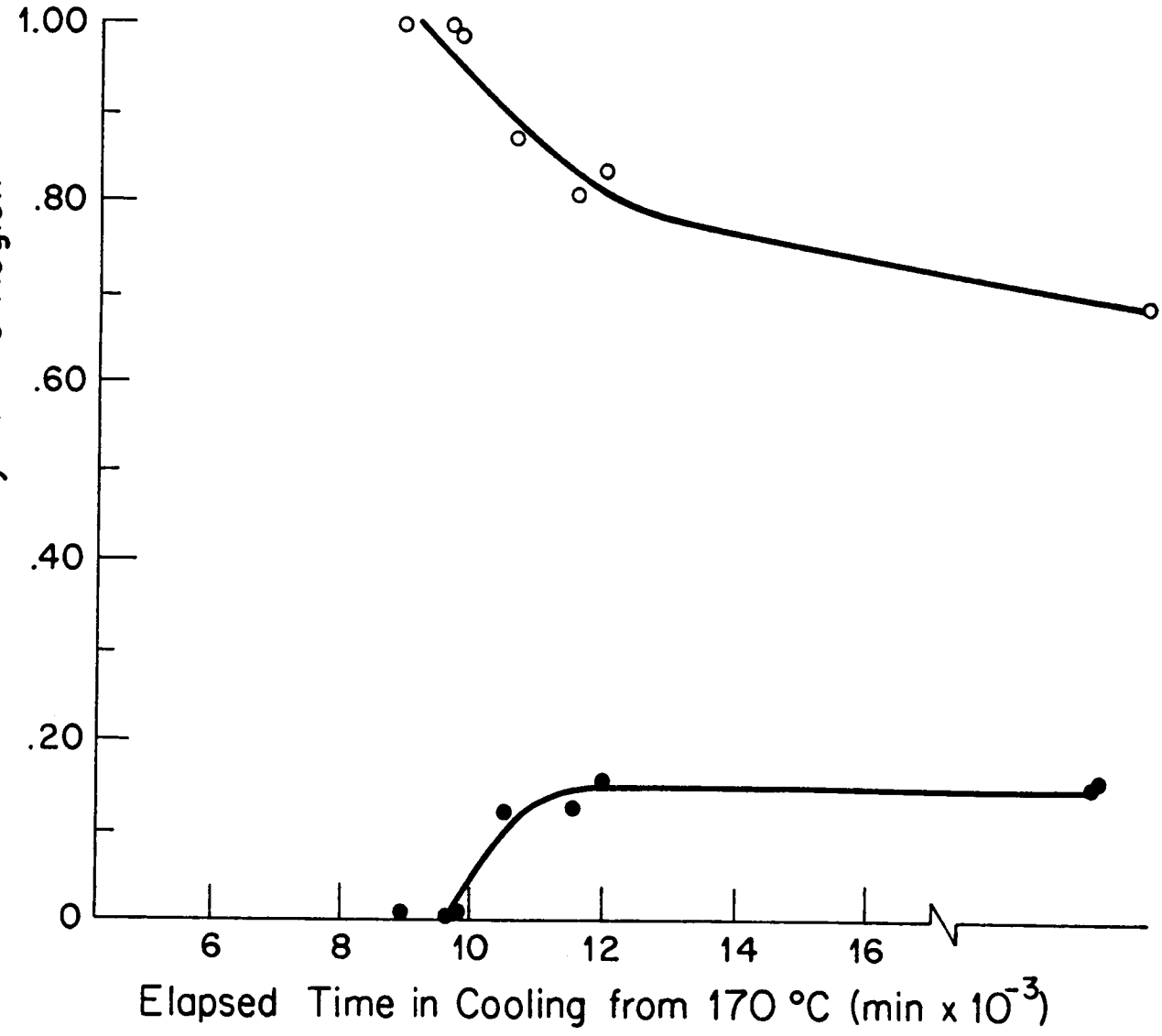

Figure 31. Relative Amount of Primary (C-Axis Oriented) and Secondary (A-Axis Oriented) Material as a Function of Spinline Residence Time (Melt Temperature 200°C, TUV 200 m/min).

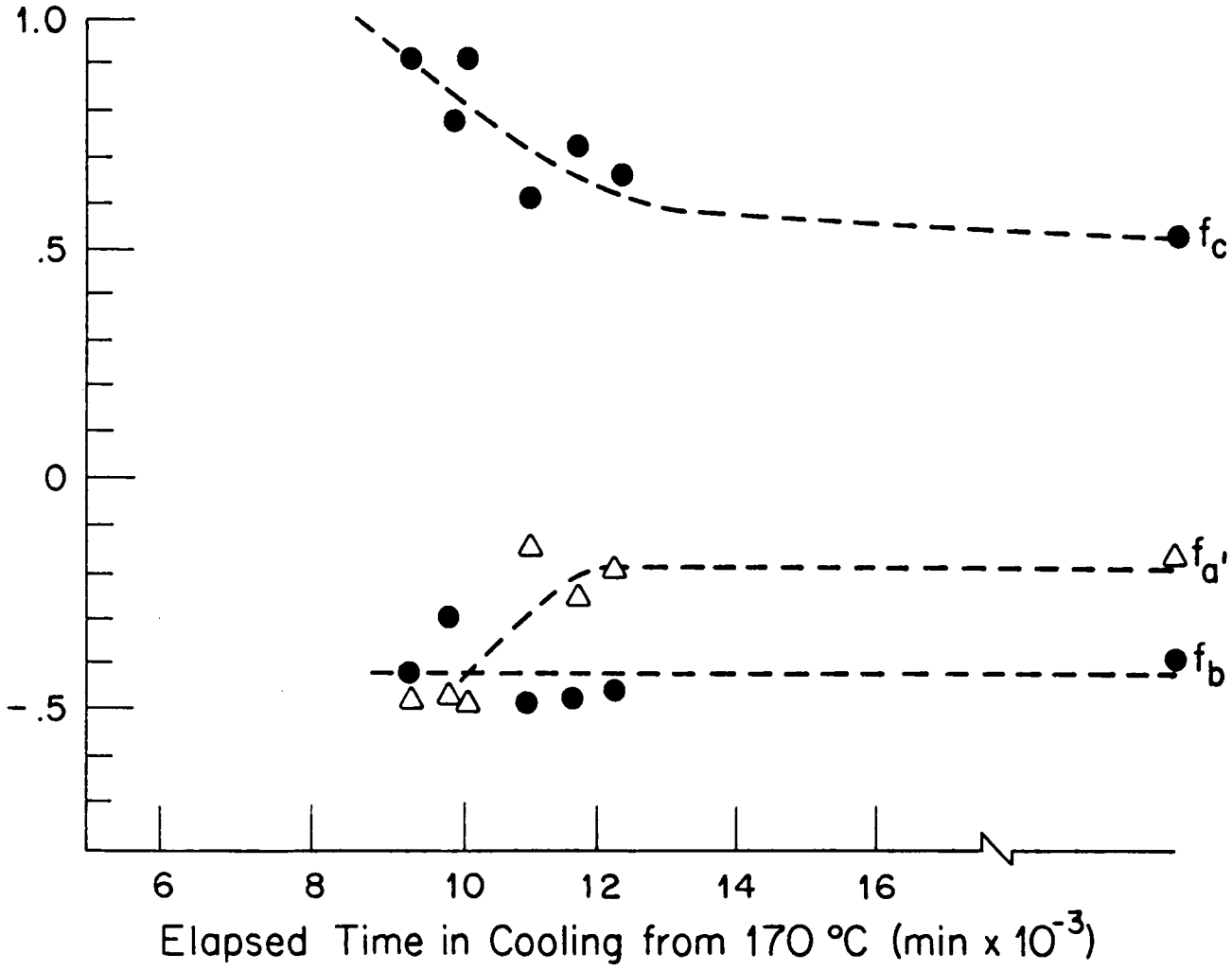

Figure 32. On-Line Development of Crystalline Orientation (Melt Temperature 200°C, TUV 200 m/min).

These lamellae grow with the c-axis perpendicular to the broad surface of the lamellae with the growth axis of the lamellae parallel to the a' axis of the unit cell. Rejected lamellae crystallize in a second stage upon the fold surfaces of the primary lamellae. This structure is shown in Figure 33.

C. DISCUSSION OF RESULTS

As-Spun Fiber Structure

Our data show a strong correlation between both the overall chain orientation developed in the fiber and that developed in the crystalline regions with nominal spinline stress. In terms of fiber morphology our interpretation follows:

1. At low spinline stresses, the structure is essentially spherulitic. The Debye rings on the wide angle diffraction patterns exhibit uniform intensity (i.e., there are no azimuthal maxima or minima). The same is true of the small angle scattering peak due to the lamellar structure, and the overall birefringence of the fiber is very low.
2. As stress is increased, however, the b axis becomes oriented normal to the fiber axis, while the c and a' axes retain a more random orientation. In this transition region the structural factors we observed could be interpreted as either the flattened spherulite described by Samuels, as well as Baranov and Volkov (39), or a poorly developed row structure, with considerable lamellar irregularities, such as that described for polyethylene (51).

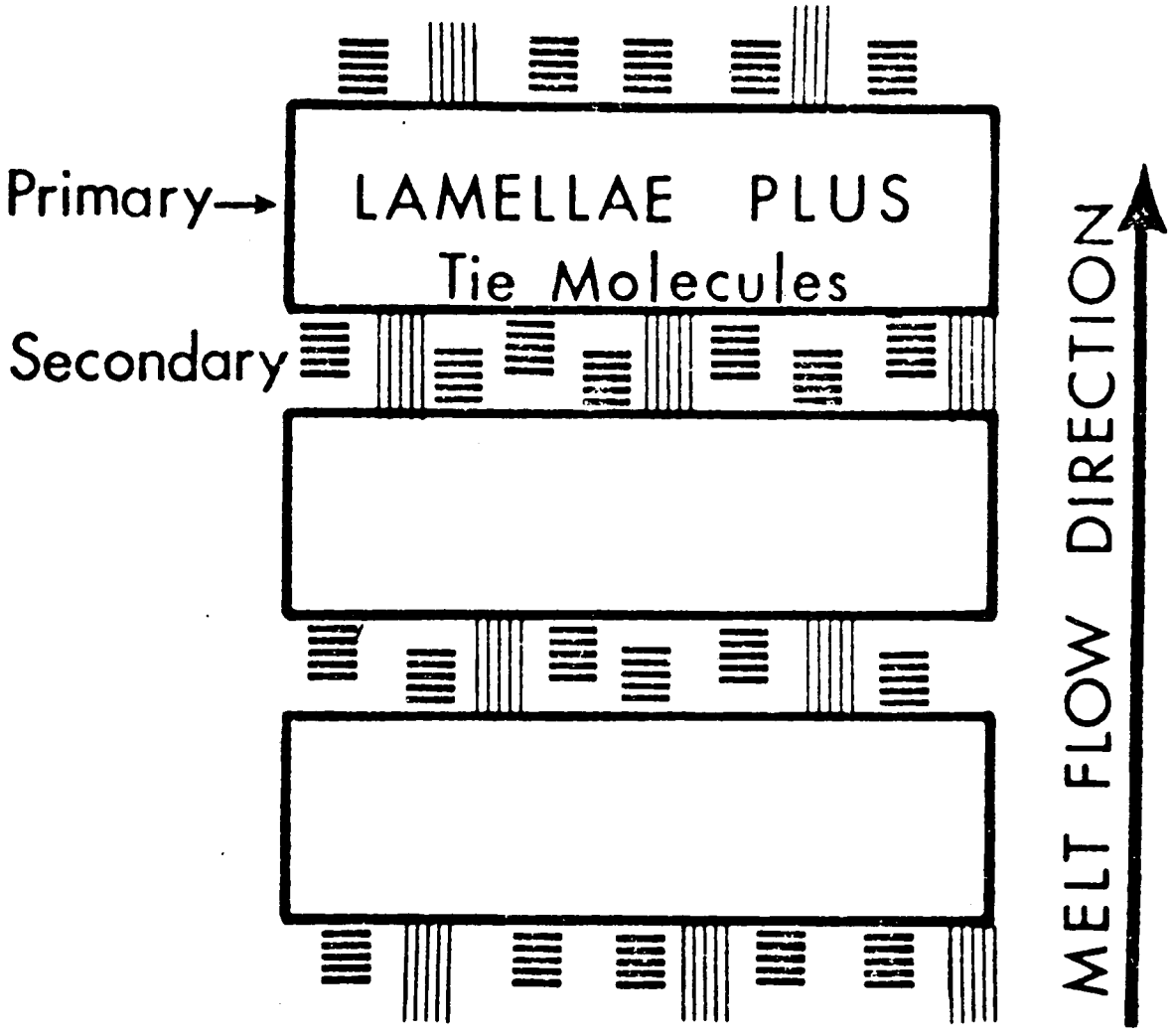

Figure 33. Morphology of Polypropylene Melt Spun at High Stress.

Source: Clark and Spruiell (12)

3. The a and c axes show a somewhat more random distribution than that reported in the case of linear polyethylene. They are also more random than for the b-axis (which rapidly becomes perpendicular to the fiber axis). This may be indicative of residual lamellar twisting or tilting at high stress levels but is more likely a result of the bimodal orientation which develops. The latter interpretation is supported by the calculations of the orientation function after separating out the a-axis contribution.

This stress-related model correlates well with elastic recovery data. The transition from spherulitic to row structure is in the same region that the fiber reaches its limiting value of elastic recovery after annealing, agreeing with the considerable work published by Clark and Sprague associating the row structure with high elasticity.

No nominal stress levels are reported in the work of Baranov and Volkov or that of Samuels, but Baranov and Volkov describe the flattened spherulites as appearing at lower melt-draw ratios, and thus lower stresses, than the oriented phase. Their description of it as an entity separate from the flattened spherulites is consistent with Keller's theory of a nucleation mechanism for the formation of row structure.

Structure Development on the Spinline

The spinline results are qualitatively similar to those obtained when observing polyethylene. Stress is seen to drastically increase the rate of crystallization, as well as orientation development on the spinline.

At relatively high spinline stress levels the first crystals to form are seen to have the high c-axis orientation of a well-developed row structure. A subsequent decrease in crystalline orientation is probably due to both a decrease in stress-produced orientation in the primary row-structure component as the developing structure supports the load as well as epitaxial growth of the secondary component.

CHAPTER V

CONCLUSIONS

A. AS-SPUN FILAMENTS

Our melt spun polypropylene fibers may be characterized as spherulites when spun at low spinline stress. Orientation functions show random orientation of the crystallographic axes, birefringence measurements indicate that chains in the amorphous regions, as well as in the crystalline, have little preferred orientation. Small angle x-ray scattering patterns show lamellar surface arranged in random manner. The fibers display mechanical properties typical of "cold drawable" polypropylene.

With increasing spinline stress the development of row structure morphology correlates with a change to "hard elastic" mechanical properties. Polymer chains in both the crystalline and amorphous regions assume orientations tending to parallel to the fiber axis, as indicated by WAXS and birefringence data. Small angle x-ray scattering patterns showed meridional maxima characteristic of lamellae stacked perpendicular to the fiber axis.

However our fibers showed bimodal orientation; i.e., a fraction of the crystalline a-axes become oriented perpendicular to the fiber axis at high spinline stress. X-ray scattering and birefringence contributions from this component mask the rather highly oriented structure

developed in our fibers. Our data supports the model for highly elastic polypropylene fibers developed by Clark and Spruiell.

B. ON-LINE STUDIES

Our on-line spinning studies showed that, at high spinline stress, the first crystallization observed on the spinline consisted of highly oriented (chains parallel to fiber axis) crystallites. More random orientation was observed as crystallization progressed, in a manner similar to that observed by Dees and Spruiell (14, 15) for a polyethylene spinline.

Varying melt temperature and fiber take-up velocity affected both spinline stress and cooling rate. Both stress and cooling rate were shown to affect crystallization kinetics. These could be discussed in terms of constant cooling transformation curves. Overall crystallization kinetics measured on the spinline were greatly enhanced in comparison to solidification under quiescent conditions.

LIST OF REFERENCES

LIST OF REFERENCES

1. Abbott, L. E. and J. L. White, Appl. Poly. Sympos., 20, 247 (1973).

2. Acierno, D., J. N. Dalton, J. M. Rodriguez and J. L. White, J. Appl. Polym. Sci., 15, 2395 (1971).

3. Addink, E. J. and J. Beintema, Polymer, 2, 185 (1961).

4. Bankar, V. G., J. E. Spruiell and J. L. White, J. Appl. Polym. Sci., 21, 2135 and 2341 (1977).

5. Baranov, V. G., T. I. Volkov, G. S. Farshyan, S. Y. Frenkel, J. Polym. Sci., C, 30, 305 (1970).

6. Beck, H. N. and H. D. Ledbetter, J. Appl. Polym. Sci., 9, 2131 (1965).

7. Binsbergen, F. L., Nature, 211, 516 (1966).

8. Binsbergen, F. L. and B. G. M. Delange, Polymer, 11, 253, 309 (1970).

9. Carothers, W. H. and J. W. Hill, J. Am. Chem. Soc., 54, 1579 (1932).

10. Clark, E. S. and C. A. Garber, Intern. J. Polymeric Mater., 1, 31 (1971).

11. Clark, E. S. in Structure and Properties of Polymer Films, Plenum Pub., New York (1972).

12. Clark, E. S., and J. E. Spruiell, Polym. Eng. Sci., 16, 176 (1976).

13. Cormia, R. L., J. Chem. Phys., 37, 1933 (1962).

14. Dees, J. R., Ph.D. dissertation, University of Tennessee, Knoxville (1974).

15. Dees, J. R. and J. E. Spruiell, J. Appl. Polym. Sci., 18, 1053 (1974).

16. Devoy, C., and L. Mandelkern, J. Chem. Phys., 37, 3827 (1970).

17. Flory, P. J., Principles of Polymer Chemistry, Cornell University Press, New York (1953).

18. Fung, P. Y. F. and S. H. Carr, J. Macromol. Sci.-Phys., B6(4), 621 (1972).

19. Fung, P. Y. F., E. Orlando, and S. H. Carr, Polym. Eng. Sci., 13, 295 (1973).

20. Geil, P. H., Polymer Single Crystals, Krieger, New York (1963).

21. Haas, T. W. and B. Maxwell, Polym. Eng. Sci., 9, 225 (1979).

22. Hock, C. W., J. Polym. Sci. Pt. 2, 5 (3), 471 (1967).

23. Hoshino, S., J. Powers, D. G. LeGrand, H. Kawai, and R. S. Stein, J. Polym. Sci., 58, 185 (1962).

24. Kardos, J. L., A. W. Christiansen, and E. Bauer, J. Polym. Sci. A2, 4, 5, 777 (1966).

25. Katayama, K, T. Amano, and K. Nakamura, Kolloid Z. Z. Polum., 226, 125 (1968).

26. Katayama, K., K. Nakamura, and Y. Takeichi, Prep A6.5, IUPAC, Intern. Symp. on Macromol. Chem., Toronto (1968).

27. Kase, S. and T. Matsuo, J. Polym. Sci., A3, 2541 (1965).

28. Keith, H. D., F. J. Padden Jr., N. M. Walter, and H. W. Wyckoff, J. Appl. Phys., 30, 1479, 1485 (1965).

29. Keith, H. D. and F. J. Padden, Jr., J. Appl. Phys., 35, 1270 (1964).

30. Keller, A. and M. Machin, J. Macromol. Sci. Phys., B1, 41 (1967).

31. Khoury, F., J. Res. NBS, 70A, 29 (1966).

32. Kitao, T., S. Ohya, J. Furnkawa, and S. Yamashita, J. Polym. Sci., 11, 1091 (1973).

33. Mandelkern, L. and F. A. Quinn, J. Appl. Phys., 25, 830 (1954).

34. Mandelkern, L. and F. A. Quinn, J. Appl. Phys., 26, 443 (1955).

35. Nadella, H. P., M.S. Thesis, University of Tennessee, Knoxville.

36. Nadella, H. P., H. M. Henson, J. E. Spruiell, and J. L. White, J. Appl. Polym. Sci., 21, 3003 (1977).

37. Natta, G. and P. Corradini, Nuovo Cimento Suppl., 15, 40 (1960).

38. Noether, H. D. and W. Whitney, Kolloid-Z.-Z. Polym., 251, 991 (1973).

39. Ruland, W., Acta Cryst., 14, 1180 (1961).

40. Samuels, R. J., J. Polym. Sci., 20, 253 (1967).

41. Samuels, R. J., J. Polym. Sci., A2, 6, 2021 (1968).

42. Samuels, R. J., J. Polym. Sci., A1, 1741 (1965).

43. Sauer, J. A., D. R. Morrow, and G. C Richardson, J. Appl. Phys., 36, 3017 (1965).

44. Sharples, A. Introduction to Polymer Crystallization, St. Martin's Press, New York (1966).

45. Sheehan, W. C., and T. B. Cole, J. Appl. Polym. Sci. 8, 2359 (1964).

46. Shii, H. and K. Ishikawa, Reports on Polymer Physics in Japan, 13, 131 (1970).

47. Sprague, B. S., J. Macromol. Sci., Phys., B8(1-2) 157 (1973).

48. Spruiell, J. S. and J. L. White, Ploym. Eng. Sci., 15, 660 (1975).

49. Turnbull, D., J. Chem. Phys., 18, 198 (1950).

50. Turner Jones, A., J. J. Aizlewood and D. R. Beckett, Makromol. Chem., 75, 134 (1964).

51. Volkov, T. I., Vysokomol. Soyed All., Polymer Sci. USSR, 108 (1969).

52. Weidinger, A., and P. H. Hermans, Makromol. Chem., 50, 90 (1961).

53. White, J. L., J. Appl. Polym. Sci., 8, 2239 (1964).

54. White, J. L., K. C. Dharod, and E. S. Clark, J. Appl. Polym. Sci., 18, 2539 (1974).

55. Wilchinsky, Z. W., J. Appl. Phys., 30, 792 (1959).

56. Wilchinsky, Z. W., J. Appl. Phys., 31, 1969 (1960).

57. Wilchinsky, Z. W., Adv. X-Ray Anal., 6, 231 (1963).

58. Wilchinsky, Z. W., J. Polym. Sci., A2, 281 (1968).

59. Yamamoto, M. and J. L. White, J. Polymer Sci. A-2, 9, 399 (1971).

60. Ziabicki, A., and K. Kedzierska, Kolloid-Z., 175, 14 (1961).

61. Ziabicki, A., Appl. Polym. Symposia, 6, 1 (1967).

62. Ziabicki, A., in Man Made Fibres, Vol. I, H. Mark, S. M. Atlas, and E. Cernia, Eds., Wiley, New York, 1967.

VITA

Helen Mateer Henson was born in Hamilton, Ontario, Canada, on April 4, 1944. She attended elementary and high schools in that country. In 1962 she entered the University of Kentucky, and in June 1966 received a Bachelor of Science degree in Physics.

She was employed by Oak Ridge National Laboratory from 1966 to 1973, when she entered the Graduate School at The University of Tennessee. She received the Master of Science degree with a major in Metallurgical Engineering in December 1979. She has been employed by Union Carbide Corporation, Nuclear Division, since December 1974.

She is married to Tommy Joe Henson of Clinton, Tennessee.